Journal of Science: Advanced Materials and Devices 9 (2024) 100778

Contents lists available at ScienceDirect

Journal of Science: Advanced Materials and Devices

journal homepage: www.elsevier.com/locate/jsamd

Review Article

Printing of passive RFID tag antennas on flexible substrates for long read distance applications: Materials and techniques ☆

Mohd Nizar Hamidon [a,*], Tark D. Farnana [a], Intan H. Hasan [a], Aduwati Sali [b], Maryam Md. Isa [b]

[a] Institute of Nanoscience and Nanotechnology, Universiti Putra Malaysia, UPM Street, Serdang, 43400, Selangor, Malaysia
[b] Faculty of Engineering, Universiti Putra Malaysia, UPM Street, Serdang, 43400, Selangor, Malaysia

ARTICLE INFO

Keywords:
Conductive ink
Flexible electronics
Inkjet printing
Screen-printing
Electroless plating
Passive RFID tag antenna
Wearable antenna
E-textile

ABSTRACT

Radio frequency identification (RFID) is an emerging technology that has a crucial role in many areas. To be suitable for these applications, RFID tags must be flexible, which presents greater manufacturing challenges. Printing as an additive manufacturing method is preferred over subtractive processes due to its efficient use of materials and environmental friendliness. This review presents key properties of the printed patterns, namely electrical conductivity, layer thickness, and surface morphology. It links them to the reading distance between the RFID tag and the reader. The types of conductive inks and their role in achieving a long-read distance of flexible antennas are also discussed. The properties of flexible substrates linked to the printing process are also presented. These substrates were classified into paper, polymer, and textiles. This article considers two laboratory-scale printing techniques commonly used in research: inkjet and screen printing. The printing parameters of these printing techniques that affect the printing quality are covered. Furthermore, electroless plating is presented as a metallization process or a complementary method to other printing techniques.

Contents

☆ This work is fully funded by Universiti Putra Malaysia UPM, under grant number GP-IPS/2023/9748900. And the work was carried out in the Institute of Nanoscience and Nanotechnology ION2, UPM, as part of project No. 9748900.

* Corresponding author.
E-mail addresses: mnh@upm.edu.my (M.N. Hamidon), tarkfarnana@gmail.com (T.D. Farnana), i_helina@upm.edu.my (I.H. Hasan), aduwati@upm.edu.my (A. Sali), maryam@upm.edu.my (M.M. Isa).

Peer review under responsibility of Vietnam National University, Hanoi.

https://doi.org/10.1016/j.jsamd.2024.100778
Received 7 February 2024; Received in revised form 10 August 2024; Accepted 18 August 2024
Available online 22 August 2024

1. Introduction

Radio frequency identification RFID is a rapidly evolving technology. The RFID system consists of a tag, reader and computer. The antenna is the main part of the tag. Passive RFID tags are preferred over active ones because they are battery-free, durable, and more cost-effective. If the tag does not contain a chip, it is called a chipless RFID tag. RFID system applications start from a barcode replacement [1–4] to more complex applications such as tracking [5], positioning [6], access control systems [7] and toll systems [8]. Moreover, it became a part of many areas from the Internet of Things (IoT) [9,10], wireless sensor networks (WSN) [11–13], food industry [14–16] and construction industry [17,18], and medical applications [19,20]. Most of these applications require a long tag-reader communication distance.

In the past, tags were fabricated on rigid substrates. However, flexible and wearable tags are becoming increasingly popular today because they are cost effective, lightweight, smaller, highly customizable, and integrable with many applications [21]. Flexible tags use flexible materials such as paper, polymer films, and textiles as a substrate, which brings additional fabrication challenges and restricts the ink type and formulation [21]. For instance, wearable textile tags introduce additional challenges to ink formulation, as the ink must be stretchable, highly flexible, and washable for durability [22].

Fabrication processes that are safe for the environment, wise usage of materials, and low-cost devices have become urging in recent years. Printing as an additive manufacturing technique is the key to realizing low-cost and environment-friendly RFIDs. Printing is advantageous over-etching — the subtractive manufacturing technique that involves a massive waste of chemicals that are usually harmful to the environment [23–25]. There are various printing techniques for printed electronics, such as: screen printing, gravure printing, flexographic and offset printing, inkjet, aerosol jet, electrohydrodynamic jet [26–28]. The selection of a printing method for RFID depends on several factors, such as print quality, throughput, resolution and achievable thickness. The commonly used printing techniques in research are inkjet printing [29,30] and screen printing [31]. Inkjet and screen printing offer better print quality than gravure, offset and flexographic printing, their precession is lower than that of new printing techniques such as aerosol and electrohydrodynamic jet printing [28]. When it comes to cost, scalability, ease of use and the thickness of the printed layer, inkjet and screen printing offer a more balanced approach, making them viable options for mass production of RFID antennas. Electroless plating is used as a metallization process for heat-sensitive substrates [32] or as a complementary process to other printing methods due to its excellent print layer properties [33–35].

To the best of the authors' knowledge, no review paper covers the RFID tag antenna printing process. Furthermore, there is a lack of review papers that link the RFID tag antenna performance to the ink and substrate properties and the printing quality. This paper aims to fill this gap; it focuses on printing UHF tag antennas on flexible substrates and relates the antenna performance with the printed layer properties. It considers two laboratory-scale additive printing techniques most used in research: inkjet printing and screen printing. The suitable flexible substrates, their properties, and treatment methods to improve printing quality are included. Post-printing processes, such as sintering, are out of the scope of this paper. However, it is worth mentioning that there are several sintering methods, namely thermal, laser, infrared, plasma, microwave, and electrical [36,37]. Since thermal sintering is mainly used for its reliability, low cost, and ease of use [23], we review works that use it as a post-processing method.

This paper is divided into four sections: The first section relates antenna efficiency to the properties of the printed conductive layer, including its conductivity, thickness, and surface morphology. The second section introduces conductive inks, which are divided into five subsections: metal nanoparticle inks, metal particle-free inks, polymer-based inks, and carbon-based inks, and the last subsection discusses the effect of ink type on the read distance between the tag and the reader. The third section covers flexible substrates, classified into three types: paper, polymer, and textile. The additional subsection discusses substrate wettability. Finally, three printing techniques are discussed: inkjet printing, screen printing and electroless plating.

2. Effect of the conductive printed layer properties on the tag antenna performance

The read distance is the most crucial characteristic of the RFID tag performance, especially for IoT, wireless sensor networks WSNs, road tolls, indoor localization, and medical applications. The read distance d can be estimated using the formula

$$d = \frac{\lambda}{4\pi}\sqrt{\frac{P_r G_r G_t \tau}{P_{th}}} \tag{1}$$

where λ is the wavelength, P_r and G_r are the transmitted power by the reader antenna and its gain, respectively, G_t is the gain of the tag antenna, P_{th} is the minimum threshold power required to power the RFID ASIC (Application Specific Integrated Circuit) chip of the tag, and τ is the power transmission coefficient, which indicates the impedance match between the tag antenna ($Z_A = R_A + jX_A$) and the RFID chip ($Z_C = R_C + jX_C$) [38,39], and defined as:

$$\tau = \frac{4R_C R_A}{|Z_C + Z_A|^2} \quad , \quad 0 \geq \tau \geq 1 \tag{2}$$

From Eq. (1), the read distance determined by the product $P_r G_r$ is known as the effective isotropic radiated power $EIRP$ of the reader. The $EIRP$ factor must not exceed the maximum value regulated by authorization organizations of each country. Moreover, $G_t \tau / P_{th}$ called the tag sensitivity $P_{th,tag}$ [40]. P_{th} value is provided by the chip manufacturer, τ can be maximized by careful design of the antenna to match the chip to its optimum value $\tau = 1$, and G_r is highly dependent on the conductivity of the antenna structure. Read distance also depends on the radiation patterns and polarization of the reader and the tag antenna [41].

In order to understand the impact of the tag antenna gain on the communication distance between the tag and the reader, practical values of the parameters in Eq. (1) are substituted as follows: $EIRP = P_t G_t = 4$ watt (this is the standard value in the USA, Japan, and India. Other countries specify other values around this), $\tau = 1$ for the tag antenna is assumed to be fully matched to the chip, and ASIC chips with $P_{th} = -18$ dBm is commercially available, the operating frequency $f = 915$ MHz is the mid-frequency of the allocated spectrum for UHF RFID. The read distance d will be

$$d = 13.1\sqrt{G_t} \tag{3}$$

Because Eq. (1) does not consider losses due to polarization mismatch, tag-to-reader orientation, packaging, communication medium attenuation, and materials to which the tag is attached. Nevertheless, Eq. (3) gives more understanding of the dependence of the read distance on the tag gain. The antenna gain depends on its efficiency η_r and directivity D, as follows.

$$G = \eta_r D \tag{4}$$

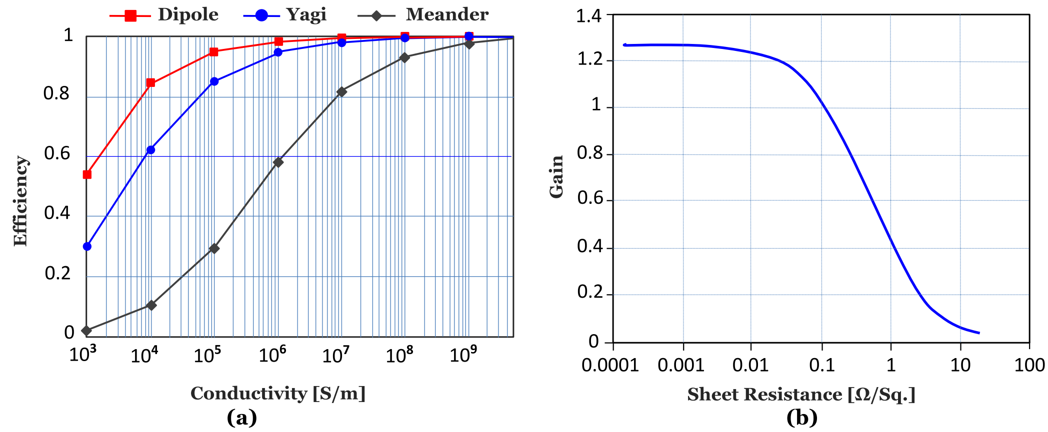

Fig. 1. Effect of the electrical conductivity on the antenna gain. (a) The antenna efficiency versus the conductivity of its structure. Reproduced with permission [42], 2015, IEEE. (b) Dependence of the antenna gain on the sheet resistance. Reproduced with permission [45], 2016, IEEE.

The subsequent subsections discuss the properties of the printed layer that influence antenna efficiency and gain. These properties are the printed pattern's conductivity, thickness, and surface morphology.

2.1. Conductivity of the printed pattern

The impact of the conductivity of the antenna structure on its radiation efficiency was studied by Shahpari et al. [42]. Three wire antennas in free space, dipole, Yagi-Uda, and meander, have been simulated using FEKO EM software. Fig. 1(a) depicts the dependence of the efficiency on the conductivity. As can be seen clearly from Fig. 1(a), the meander antenna is more sensitive to reduced conductivity than the other two antenna types. The three antennas were fabricated from brass and graphite, and the measurements agree with the simulated results. These findings agree with the measured results by [43,44]. The effect of the sheet resistance R_{sh} of the printed layer of the antenna on its gain and impedance matching has been studied by [45], the study carried out by simulation of a half-wave dipole antenna with impedance matching loop using QuickWave-3D electromagnetic solver. The antenna designed for UHF RFID tags operates at 915 MHz. Fig. 1(b) shows the antenna gain's dependence on the antenna structure's sheet resistance

2.2. Thickness of the printed layer

Merilampi et al. [46] conducted a study on the effect of conductive ink thickness on the performance of the printed tag antenna. At high frequencies, the current density J at the surface has the highest value J_o, and decreases exponentially inside the conductive layer.

$$J(z) = \sigma E_o e^{-z/\delta} = J_o e^{-z/\delta} \quad , \quad J_o = \sigma E_o \quad , \quad \leq z \leq t \tag{5}$$

where σ is the conductivity of the printed layer, E_o is the electric field intensity at the surface, z is the depth from the surface, t is the substrate thickness, and δ is the skid depth defined as:

$$\delta = \frac{1}{\sqrt{\pi f \mu \sigma}} \tag{6}$$

where μ is the magnetic permeability.

The optimum thickness of the printed layer must be determined for efficient use of the conductive ink. A thin layer less than δ will introduce high resistivity, leading to higher ohmic losses and reducing the antenna's radiation efficiency. Furthermore, over-thickening will not introduce noticeable improvement because the current density far from the surface is negligible. Thus, it is a waste of material to over-thicken the printed layer. Therefore, it is crucial to determine the minimum thickness to guarantee a good enough conductivity to provide the required antenna efficiency. In the mass production of RFID antennas, saving small amounts of ink per antenna can save thousands of dollars daily. The efficient use of conductive materials can achieve this; the antenna thickness varies according to the current density distribution. Higher current density regions are thicker than low current density [47]. The sheet resistance of the printed layer as a function of σ, δ and the layer thickness t is

$$R_s = \frac{1}{\sigma\delta}\left(1 - e^{-t/\delta}\right)^{-1} \tag{7}$$

The antenna's radiation efficiency depends on the radiated power and the power loss as follows.

$$\eta_r = \frac{P_r}{P_l + P_r} = \frac{R_r}{R_l + R_r} \tag{8}$$

where P_l is the total loss by the ohmic resistance and the dielectric loss power due to the substrate, and P_r is the radiated power.

Merilampi et al. simulated three quarter-wave dipole antennas to resonate at 866 MHz, with an identical geometry except for the conductive layer thickness. The estimated skin depth was $\delta = 15$ μm. The three thicknesses used were $t_1 = 13.9$μm, $t_2 = 21.5$μm, and $t_3 = 51.5$μm, which are equivalent to 0.93 δ, 1.43 δ, and 3.43 δ respectively, to confirm the theoretical analysis. The substrate was Polyethylene naphthalate PEN, and then it was simulated in free space to compare the losses due to the substrate to the ohmic resistance losses. Fig. 2(a) shows that the loss resistance decreases with the thickness increase, and Fig. 2(b) shows a significant improvement in the antenna efficiency by increasing the thickness. As it is apparent, the contribution of substrate losses is minor compared with ohmic losses, and the radiation efficiency is slightly reduced when PEN substrate is added. As a result, the antenna gain will increase with the increase in radiation efficiency, according to Eq. (4).

In addition, the three antennas were screen-printed on a PEN substrate and assembled with an RFID chip to form a tag. Then, the scattered power from the tag is measured versus the power transmitted by the reader, as shown in Fig. 2(c). As expected, the tag with the thickest antenna scattered the strongest power.

2.3. Surface morphology

Normally, the printed patterns suffer from different defects depending on the fabrication method [41]; for instance, the uneven layer is associated with screen printing, as shown in Fig. 3(a). Assuming a draw of a part of a printed conductive layer shown in Fig. 3(b), the height h changes only in the direction of the current flow. By dividing the layer into incremental slices, the resistance of each slice is R_i, where

$$R_i = \frac{\Delta L}{\sigma W h_i} \tag{9}$$

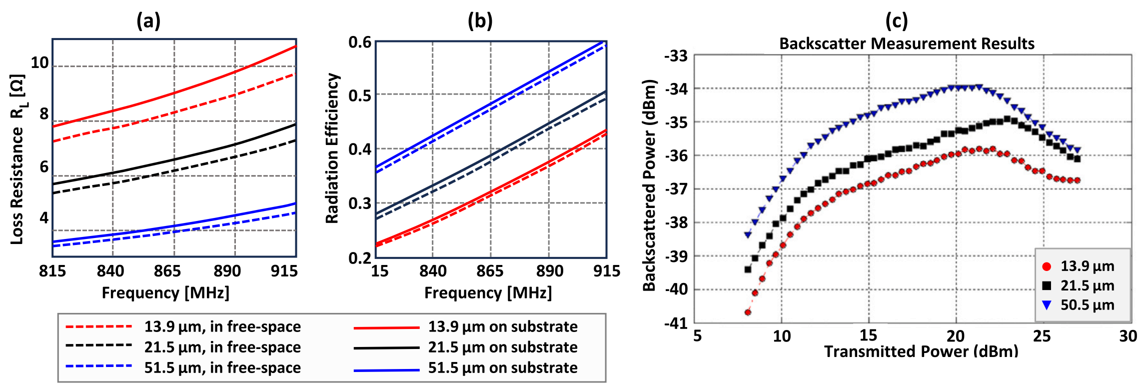

Fig. 2. The performance of three screen-printed quarter wave dipoles for UHF RFID with different thicknesses 13.9 μm, 21.5 μm, and 50.5 μm. (a) Simulated loss resistance. (b) Simulated radiation efficiency. (c) Measured backscattered signal power versus the transmitted power.
Source: Reproduced with permission [46], 2010, IEEE.

All resistances are connected in series, thus the total resistance R_T is

$$R_T = \sum_{i=1}^{N} \frac{\Delta L}{\sigma W h_i} = \frac{\Delta L}{\sigma W} \sum_{i=1}^{N} \frac{1}{h_i} \tag{10}$$

This relationship shows that the rate change of R_T with respect to h is greater for minimum values of h than the maximum values. This means that the average value of the printed layer thickness t is not accurate enough to estimate the equivalent value of h. Instead, the standard deviation is a more accurate tool and more suitable for evaluating the impact of the surface morphology on the total resistance. It is clear that the smaller the standard deviation (smoother surface), the lower the total resistance. This analysis is for DC, and the situation is much worse for ultra-high frequency current because the current density is high in a region near the surface, according to Eq. (5).

Two roughness descriptors are recommended by the International Standardization Organization (ISO) and the American National Standards Institute (ANSI). These descriptors are center line average roughness R_a and root mean square roughness R_q, which are defined over sample length L by Eq. (11) and Eq. (12), respectively.

$$R_a = \frac{1}{L} \int_0^L |Z(x)|\, dx \tag{11}$$

$$R_q = \sqrt{\frac{1}{L} \int_0^L [Z(x)]^2\, dx} \tag{12}$$

where $Z(x)$ is the height of the surface above the mean line at a distance x from the origin [48,49].

When the printed layer is very thin, the uneven distribution of the ink becomes evident, as noticed in the gravure-printed tag. The impact of such a defect on the performance is evident in small traces with high current densities, like the matching loop of a produced tag [41]. The two mass-production printing techniques, gravure and flexography suffer from uneven printed film, especially for narrow traces of width 1 mm or less, which can become rough compared with other techniques. This will severely degrade the conductivity, which may lead to non-conductive traces for narrow traces printed perpendicular to the printing direction [41,47]

Also, the substrate roughness has a large influence on the overall resistance of the printed films. Morais et al. printed PEDOT:PSS polymer-based ink on three different substrates: bond paper, vegetal paper, and PET film. The measured sheet resistance Rsh and the substrate's roughness are presented in Table 1 [50]. Since the current density at the bottom of the conductive film is the same as at the top, the sheet resistance of the film is related to the surface roughness of the substrate because the smoothness of the printed film is highly dependent on that of the substrate.

Three properties of the printed structure of the antenna were discussed, and their influence on the antenna efficiency was clarified. First, antenna efficiency was found to be very sensitive to the conductivity of its structure. Second, the efficiency was significantly improved as its thickness increased to approximately 3.5 times its skin depth. Finally, the smooth surface of the printed antenna is important to maintain its high efficiency.

Table 1
Measured sheet resistance of different flexible substrates along with their roughness descriptors [50].

Substrate	R_a (nm)	R_q (nm)	R_{sh} (KΩ/sq)
Bond paper	1750	55.4	413
Vegetal paper	540	153.1	5.6
PET	730	32.7	2.3

3. Conductive ink

Conductive ink contains highly conductive material used to print the conductive parts of printed electronics, such as conductive traces, antennas, and electrodes. Conductive inks must have high electrical conductivity, good adhesion to the substrate, good dispersion, good stability and rheological properties, low sintering temperature, and low cost and environmental friendliness [26]. Textile antennas impose additional requirements on the ink; these antennas are required to be washable, more flexible, and stretchable [51,52].

Generally, conductive inks consist of four main components: conductive elements (called fillers or precursors), binders, solvents, and additives, Fig. 4. The conductive inks are divided into two types based on the form of conductive element: nanoparticle and particle-free inks. If the conductive element is in nanoparticle form, it is called a conductive filler. Examples of these fillers are metal nanoparticles, graphene, carbon nanotubes (CNT), and nanowires. The ink is called nanoparticle ink. Meanwhile, if the conductive element is in the form of a chemical compound called a precursor, the ink is called particle-free ink [53,54].

Solvents are responsible for the dispersion and dissolution of the ink components. Also, they are employed to modify viscosity and surface tension. Solvents are chosen to be volatile to evaporate completely upon heating. In the ink industry, different additives are added to modify different properties; the typical additives added to ink are surfactants, adhesion promoters, and rheology modifiers. Surfactants serve as wetting agents or dispersing agents. Adhesion promoters enhance the adhesion between the printed layer and the substrate. Rheology modifiers known as thickeners are added to alter the viscosity and other rheological properties to tailor the ink or paste for a specific printing technique or machine [55,56].

A proper ink design plays an essential role in improving printed pattern properties. It enables a highly conductive layer with a very low portion of non-conductive particles upon sintering. At the same

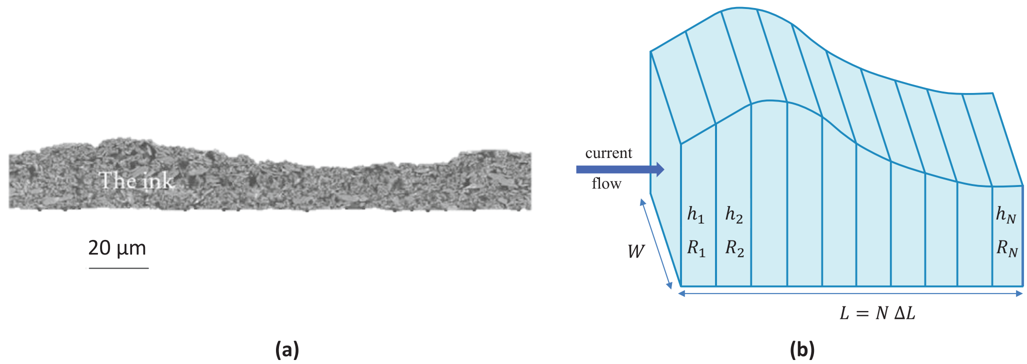

Fig. 3. Uneven printed layer thickness. (a) Scanning electron microscope micrograph of a screen-printed antenna with an average thickness of 21.5 μm. (b) Schematic diagram. *Source:* Reproduced with permission [41], 2009, Hindawi.

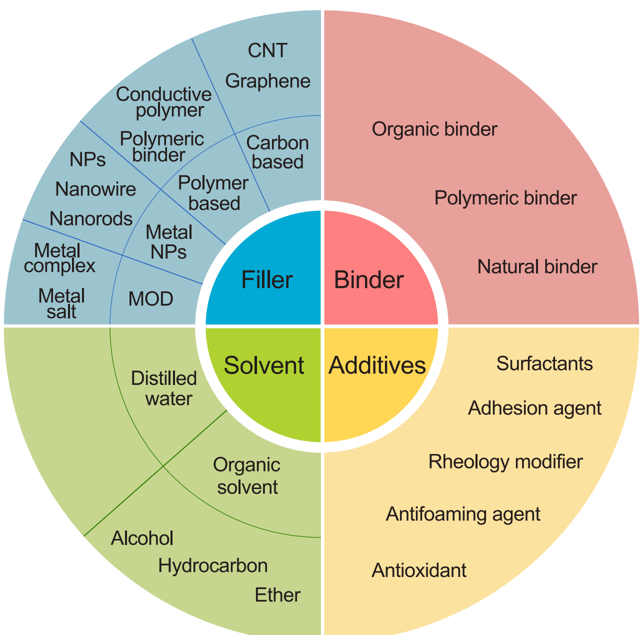

Fig. 4. Components of conductive inks.

time, it reduces the sintering temperature to a level applicable to a wide range of flexible substrates. Furthermore, it has to be compatible with the targeted printing technique and has a long shelf-life. This section is divided into three subsections: metal nanoparticle inks, metal particle-free inks, polymer-based inks and carbon-based inks.

3.1. Metal nanoparticle inks

Metal nanoparticle inks contain metal nanoparticles as conductive elements. Gold [57–61], Silver [54], copper [62–64], and nickel [65, 66] are the most utilized metals for their high conductivity, see Table 2. Gold is a nonoxidizable noble metal but is costly compared with other metals. Silver-based inks are the most developed and reported conductive ink, are the most investigated in research, and are used in the industry for printed electronics [43,67]. However, silver is an expensive metal and is not suitable for large volume production of RFID tags [37]. Also, gold and silver suffer from high electromigration that can affect the durability of printed circuits if they include narrow-width traces. A major challenge in this field is to find inexpensive alternatives to expensive noble metals.

A wide range of metal nanoparticle inks has recently been developed to replace gold and silver inks, including copper NPs ink [68],

Table 2
Conductivity and resistivity of most used metals as a functional material for conductive inks. The conductivity values are taken from [66], and the resistivity from [75].

Material	Conductivity Sm^{-1}	Resistivity Ω.m
Silver	6.30×10^7	1.59×10^{-8}
Copper	5.97×10^7	1.68×10^{-8}
Gold	4.11×10^7	2.44×10^{-8}
Aluminum	3.77×10^7	2.65×10^{-8}
Nickel	1.43×10^7	6.99×10^{-8}

Nickel NPs ink, and core–shell NPs [69–72]. Copper NPs have issues with stability and rapid oxidation. Core–shell NPs are developed to protect easily oxidizable metals (copper and nickel) by covering them with a shell of highly oxidation-resistant metal, typically silver, to form air-stable ink.

Nevertheless, NP inks suffer from several drawbacks, such as agglomeration of the suspended particles during synthesis, printing, and storage, nozzle clogging in IJP, and high sintering temperatures (generally > 200 °C) [73]. Nanoparticle synthesis is a complex process that includes high-speed centrifugation, multiple washing steps, high vacuum drying, and high-temperature annealing [66]. The achieved conductivity of sintered nanoparticle metals are much less than that of bulk [74].

3.2. Metal particle-free inks

Metal particle-free inks are developed to solve most problems associated with utilizing NP inks. Metal particle-free inks are composed mainly of metal salts or metal complexes and solvents. The formulation of the particle-free inks is discussed in detail in [73]. They can be directly decomposed by low-temperature thermal sintering or other sintering techniques to produce pure metal, which leads to highly conductive film. These inks have attracted much attention due to their relatively low sintering temperature (< 200 °C) compared to metal nanoparticle inks 200–400 °C. Because the inks contain metals in a chemical compound, they possess excellent stability, no aggregation during preparation and storage, nozzle clogging, and a more straightforward preparation process than NP inks.

The complexing of metal salts decreases the energy required to redox reactions, leading to lower decomposition temperatures. For instance, the thermal decomposition of copper formate tetrahydrate salt was compared with the salt complexed with an n-octyl amine to examine the effect of complexing on the sintering temperature. The Thermal gravimetric TG measurement in Fig. 5(a) shows that mass loss occurs in two stages; n-octyl amine evaporates in the first stage in the 80–110 °C temperature range. The second stage occurs in the 130–140 °C temperature range when CuF decomposes sharply to

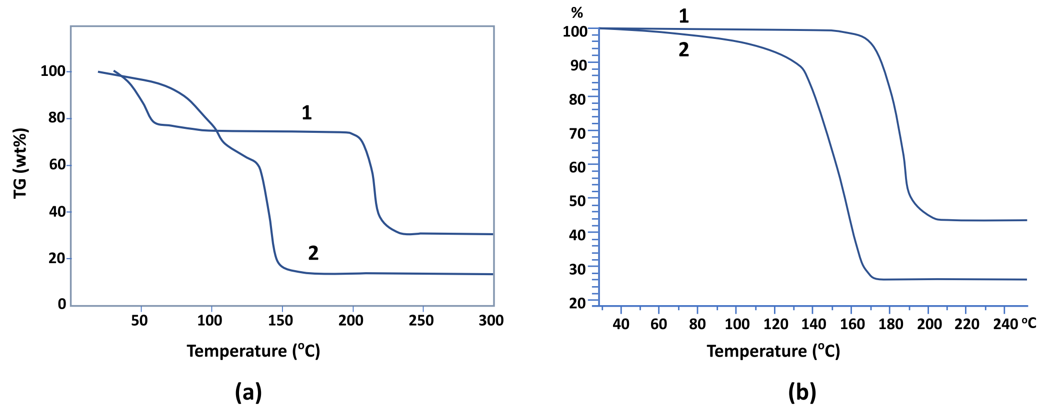

Fig. 5. The effect of the water amount in the salt on the decomposition process. (a) Mass loss in percentage of the printed ink during thermal decomposition (1) CuF tetrahydrate salt (2) CuF tetrahydrate complexed with n-octyl amine. Reproduced with permission [76], 2011 Elsevier. (b) TG analysis of the thermal composition of (1) dehydrated CuF, and (2) dihydrated CuF complex. Reproduced with permission [78], 2015, Royal Society of Chemistry.

produce pure copper. On the other hand, in the case of CuF salt, the composition stage happens in the range of 200–220 °C [76]. A similar experiment with similar results has been reported by Farraj et al. in which dehydrated CuF salt was compared with the salt complexed with 2-amino-2-methyl-1-propanol. The two inks are thermally decomposed and TG analyzed. An identical result has been obtained by [77].

In addition, the study by [76] explains the role of water in dehydrated salt by comparing the decomposition process of the complexed dehydrated salt to the use of anhydrous salt. The findings show that the water has reduced the composition temperature and motivated the complete decomposition of organic materials into gaseous by-products, which leads to higher conductivity. Although anhydrous CuF contains 13% more copper than dehydrated CuF, the latter exhibited a four times lower resistivity [78]. Thermal decomposition in the two experiments was done using nitrogen flow to prevent the oxidation of copper. From Fig. 5(a) and (b), the decomposition temperature of tetrahydrate CuF is less than dehydrated CuF. The reason behind this could be the difference in the amount of water used for salt.

The sintering temperature can be further reduced by the synergetic effect of two different chain-length amines. For example, several self-reducible Cuf-amine complex inks were formed by complexing copper formate with different alkyl amines. The results show that the use of a single alkylamine leads to reduced film resistivity with increasing chain length, as shown in Table 3, and inks formed using two types of amines with different alkyl chain lengths (short and long chains) yield lower resistivity films than inks formed with one type of these amines alone [77]. Hybrid amines not only reduce the sintering temperature but also enhance the uniformity of nanoparticles in the printed films [79] and help form a dense film structure of large particles filled with small ones [80]. Finally, it is important to select amines with low boiling temperatures for forming copper formate-amine ink for low sintering temperatures and eliminating organic residual impurities after sintering [81].

Table 4 compares the resistivity and layer thickness of some reported MOD inks that have been thermally sintered at temperatures less than 200 °C. Table 4 does not discuss the ink formulation. Because of this, the complex agents and solvents are not listed. Most of the inks were inkjet-printed on flexible substrates. Although most resistivity values are still shallow, the layer thickness is thin. The printing process must be repeated several times to have an acceptable thickness for antenna applications. Some values of the electrical properties are given in Sm^{-1} (conductivity) or resistivity in different units. In Table 4, all these values were converted into resistivity in μΩ cm for comparison purposes. Silver, copper, and nickel are the most suitable metals as conductive components in inks. As mentioned earlier, each metal has its advantages and disadvantages. One method to combine the advantages of more than one metal and to avoid or eliminate the drawbacks of each one is using hybrid inks. For instance, copper nanoparticles are covered by a thin layer of silver–a much more expensive metal, to protect them from oxidization and yield a low-cost, air-stable nanoparticle ink [69]. Similarly, nickel nanoparticles are covered by silver to form Nickel–Silver Core-Shell Nanoparticles [72].

Table 3
Resistivity of copper films produced from different Cuf-amine complex inks sintered at 200 °C for 40 min [77].

Material	Volume resistivity [μΩ. cm]
Cuf-Butyl	29.60
Cuf-Amyl	15.15
Cuf-Hexyl	11.53
Cuf-Propyl-Hexyl	10.80
Cuf-Butyl-Hexyl	9.43
Cuf-Octyl	8.32
Cuf-Amyl-Octyl	8.23
Cuf-Hexyl-Octyl	7.90
Cuf-Propyl-Octyl	7.06
Cuf-Butyl-Octyl	4.28

Recent work has been carried out to develop hybrid metal particle-free inks to improve the stability and conductivity of printed patterns at low cost and reduced sintering temperature. The idea is based on the exploitation of the catalytic property of silver to facilitate reduction and reduce the sintering temperature. By adding silver oxalate to copper formate complex ink, the sintering temperature has been reduced from 175 to 142 °C [95], and sintering at 100 °C has been achieved by adding Ag(I) β-ketocarboxylate to Cu(II) formate tetrahydrate [96]. The printed patterns showed a high oxidation resistance at a temperature of up to 140 °C and excellent stability at high humidity of 85%.

3.3. Polymer-based inks

Although metal particle-free inks yield flexible and highly conductive films [79], their flexibility is still not enough. There are applications where greater flexibility is required, especially e-textiles. Nanoparticle inks are more amenable to improving flexibility through the use of a flexible binder and the proper selection of conductive fillers and their concentration. However, this improvement comes at the cost of conductivity.

Textile antennas are prone to harsh deformation–bending and stretching, especially if the textile is more flexible and stretchable than the cured ink. Traditional conductive inks are not flexible enough to retain their electrical and mechanical properties. They tend to crack and split and eventually degenerate. To tackle this problem, an interface layer is introduced before printing the conductive pattern.

Table 4
The electrical resistivity and layer thickness of some reported MOD inks that printed and thermally sintered at low temperatures below 200 °C.

Precursor	Printing techniques	Substrate	Sintering Temp., Time	ρ[a] [μΩ cm]	t[b] [μm]	Ref.
Silver nitrate	Inkjet printing	Glass	100 °C, 60 min	13.7	0.3238	[82]
Silver nitrate	Inkjet printing	PET	150 °C, 5 min	3-4.8	NA	[83]
Silver nitrate	Inkjet printing	Silicon	90 °C, 15 min	1.6	NA	[84]
Silver nitrate	Inkjet printing	PET	150 °C, 50 min	17	0.140	[85]
Silver oxide	Inkjet printing	PET	75 °C, 20 min	6	0.15	[86]
Silver oxalate	Inkjet printing	PI	150 °C, 30 min	8.6	1.2	[87]
Silver acetate	Inkjet printing	PET	75 °C, 60 min	36.5	1.22	[88]
Silver tartrate	Inkjet printing	PET	160 °C, 10 min	4.3	NA	[89]
Silver acetate	Inkjet printing	PET	150 °C, 30 min	4.71	≈ 4[c]	[90]
Silver oxalate	Spin coating		170 °C, 20 min	6.71		[79]
Silver acetate	Inkjet	Paper	NA	83.33		[91]
Silver oxide		PI	100 °C, 40 min	16.8		[92]
Copper hydroxide	Blade coating	Glass	160 °C, 30 min	238	NA	[93]
Copper formate tetrahydrate	Squeegee coating	Glass	140 °C, 60 min	20	NA	[76]
Copper formate tetrahydrate	Spin coating	Glass	180 °C, 1 min	18	NA	[94]

[a] ρ is the electrical resistivity.
[b] t = layer thickness.
[c] After printing 7–8 times.

This layer is normally screen-printed or deposited dielectric made from polymer. Also, flexible inks have been developed for such conditions. They are conformal and resilient to deformation [97].

Polymeric inks contain polymeric binders, solvents, conductive fillers, and additives like surfactants. The rheological properties of ink depend on the composition of the polymeric matrix, temperature, filler particle size and amount. The ink can be tailored to inkjet or screen printing by controlling these parameters. There is a trade-off between electrical conductivity and ink stability. Low conductive filler content leads to excellent stability but low electrical conductivity and vice versa [51]. Conductive polymers appear to be promising materials for wearable antennas [21]. Among them, poly(3,4ethylenedioxythiophene) polystyrene sulfonate PEDOT:PSS possesses the highest maximum conductivity of 1500 S/m. Its conductivity can still be improved by adding conductive fillers such as CNT, graphene and silver nanowires [21,98].

3.4. Carbon-based inks

graphene, and carbon nanotubes CNTs are intensively investigated. These inks are low-cost, lightweight, flexible, and recyclable inks. They have been developed to replace metals in some applications. Conductive films made from graphene inks [99] or CNT inks [100] are far more flexible than those made from metal-based inks.

The use of graphene to formulate conductive inks is associated with some drawbacks and limitations, including high annealing temperature and low dispersion in water due to its hydrophobic nature [26]. The graphene forms a low percentage by weight of the graphene ink, usually less than 0.01 wt%. It requires tens of successive prints to achieve acceptable layer thickness [26,37]. For this reason, the graphene ink is not preferred for inkjet printing. Graphene ink is commonly screen-printed [45,99,101,102]. The electrical conductivity of the printed graphene pattern in [99] was 8.81×10^4 Sm^{-1}, and in [101], it was 2.15×10^4 Sm^{-1}.

Moreover, the sheet resistance of screen-printed lines of 40μm width and 25 μm thickness was $30\,\Omega.\square^{-1}$ in [102]. Although the conductivity can be enhanced by hybridization with higher conductive fillers like Ag NPs, it is still far less than the conductivity of metals. However, graphene inks are suitable for fabricating flexible and stretchable electronic devices [26]. A graphene screen-printed antenna tag for UHF RFIDs was compared with a copper antenna of the same design. The findings show that the graphene antenna has a limited communication range compared to the copper antenna [45]. Therefore, the use of graphene antenna is limited to the application where the read range is not crucial.

CNTs' strong van der Walls force causes ink agglomeration [26]. Arun has reviewed the utilization of CNTs for antenna construction. The review concluded that the electrical conductivity of single-wall CNTs (SWCNTs) and multiwall CNTs (MWCNTs) in their pristine form is insufficient to achieve the desired radiation efficiency. Some techniques enhance their conductivity, such as bundling and doping or a hybrid of these techniques [100].

3.5. Effect of ink type on the read distance

To evaluate the effect of ink type on the antenna gain and the read distance, two antennas were printed, one using PEDOT:PSS polymer ink on glass and the second using engraved bulk copper on FR-4. They achieved gains of −8.6 dB and 2 dB, respectively, and the measured read distances were 0.73 and 8.7 m, respectively. Since losses in glass substrate were found to be about the same as FR-4, the losses in the polymeric ink are about 10 dB higher than losses of bulk copper [98].

Also, a meander dipole tag antenna that operates at 900 Mhz was printed on PET films using commercial silver ink (1.6×10^6 S/m) and another one using pure copper (5.8×10^7 S/m) by etching. The findings show that the antenna fabricated from copper overperforms the antenna fabricated from silver of the same design, and the measurements show a significant difference. The antenna gains were 1.46 and 1.99 dBi, and the read range was 10 and 12 m for silver and copper antennas, respectively [43]. Another study conducted by [44] compares RFID tag antennas printed with commercial silver ink to copper-etched antennas on PET films. The results agree well with those in [43]. Furthermore, the study by [44] compared an electroless plated copper antenna with a bulk copper etched antenna. The antenna efficiency of a 4.1 μm thick deposited antenna was almost identical to that of 18 μm thick bulk copper.

The conductive ink is classified into four types depending on the conductive element. Each type has its advantages and disadvantages, and the choice depends on the application. Metal NP inks are mainly used in the ink industry. Their main disadvantages are relatively high sintering temperatures and low electrical conductivity. Since metal NP inks have a much lower conductivity than pure metal, the skin depth is much higher. And to reduce losses and achieve long-read distance, the antenna thickness should be three time the skin depth [46]. For example, in [46], the estimated skin depth of silver ink was 15 μm. As mentioned in [28], this thickness can only be achieved by screen printing. For this reason, screen printing is preferable to inkjet printing

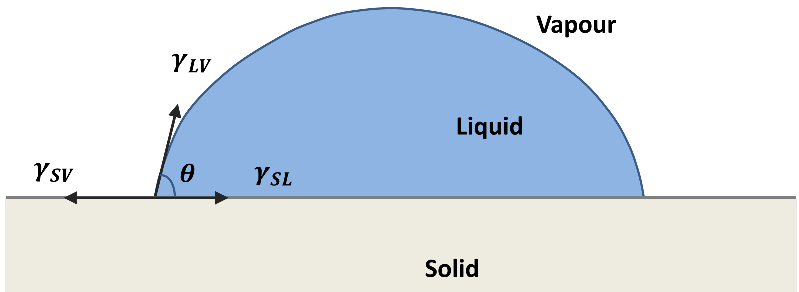

Fig. 6. A contact angle of a droplet on a solid surface.
Source: Reproduced with permission [109], 2016, IOP Publishing.

for this type of ink. Metal particle-free inks generally offer the highest conductivity compared to other types of conductive inks, and the sintering temperature is usually between room temperature and 200 °C. They are usually inkjet printed because they do not cause nozzle clogging and have a long shelf life. To obtain an acceptable thickness, the printing process must be repeated multiple times because inkjet prints a thin layer that is only about 1 μm thick [28]. Polymer-based inks are developed for wearable electronics. They offer the highest flexibility and stretchability, but their electrical conductivity values are the lowest. Carbon-based inks are the most environmentally friendly and cost-effective among other types; they are more flexible and lighter than metal inks. Their conductivity is still moderate and can be used for short-range RFID tags.

4. Substrates

In many applications, the need for flexible electronics increases continuously for its advantages over rigid substrates. Flexible antennas are used in many applications, including but not limited to RFID tags [21]. Wearable antennas are a special type of flexible antennas. It is increasingly desired in several applications, such as medical, safety, military, sports, and fitness [103]. The flexible substrates are low-cost, lightweight, stretchable, and can be mounted on curved surfaces. Different substrates are chosen for specific applications for their properties. These properties include cost-efficiency, recyclability, transparency, dielectric permittivity, piezoelectricity, biocompatibility, and environmental safety [104].

Flexible substrates must meet several requirements to be applicable for flexible electronics: high working temperature, low coefficient of thermal expansion, printability, surface smoothness, and resistance to solvents are the most important physical and chemical properties. The most utilized substrates are classified into three groups: paper, polymer and textile.

4.1. Paper substrates

Paper is a cellulose-based product derived primarily from wood pulp. Although paper is the most cost-effective and recyclable eco-friendly flexible substrate [105], its surface roughness and porosity are its most well-known disadvantages. Papers are treated by coating and calendering processes to modify their surface roughness, porosity, and surface energy for better printability. By coating or laminating with polymer materials, wax, or aluminum, the surface can be rendered impermeable to various liquids. Multilayer coating can be applied properly to achieve multiple properties [106]. Chipless RFID tags on paper are used for package tracking applications [107] and humidity sensors [108].

4.2. Polymer substrates

Various thermoplastic polymers are frequently used: Polyethylene terephthalate PET, Polyethylene naphthalate PEN, polyimide PI, Polytetrafluoroethylene PTFE (Teflon), Polyvinyl chloride PVC, and Polyvinylidene fluoride PVDF. The main disadvantage of polymer substrates is their temperature sensitivity. The maximum working temperature T_m of polymer substrates is dictated by the glass transition temperature T_g. Glass transition temperature is the temperature at which the thermoplastic polymer transits from a solid state to a rubbery state. It retains this state for various temperatures until it converts into a highly viscous liquid at melting point Tm. The main thermal properties of some of the most used polymeric substrates are presented in Table 5.

Table 5
Thermal properties of some polymers [27].

Substrate	PI	PET	PEN	TPU
T_g [°C]	155–277	70–110	120–155	80
T_m [°]C	250–452	115–258	269	180

4.3. Textile

Wearable antennas are divided by substrate into non-fabric and fabric or textile antennas. The most common textile materials used as substrates for wearable antennas are cotton, polyester, felt, fleece, silk, linen, and blended fabrics [52,110].

There are different techniques to fabricate textile antennas, but the most well-known ones are screen printing, inkjet printing, embroidery, knitting, weaving, and adhesion [51,103,110]. Every technique offers unique advantages and has its limitations and drawbacks. Most investigated textile antennas are inkjet-printed [51,97,110–112] or screen-printed [52,113,114]. Inkjet offers accuracy and ease of prototyping, while screen printing is well-suited for thick-film printing. The printing precision and quality of the screen-printed conductive layer on a textile are significantly affected negatively by the surface roughness, porosity, and surface energy of the textile [52,113,114]. Additionally, the diffusion of nanoparticles into fabric is a problem for inkjet printing [97]. Adding a suitable interface layer on top of the textile is enough to improve the printability. This layer is usually applied using screen-printable UV curable dielectric ink [110,111] or using iron-on transferable paper [97].

4.4. Wettability

The wettability of a solid surface is defined by Young's equation.

$$\gamma_{SV} = \gamma_{SL} + \gamma_{LV} \cos\theta \tag{13}$$

where γ_{SL} is solid–liquid surface tension, γ_{LV} is the liquid–vapor surface tension, and γ_{SV} solid-vapor surface free energy. Both γ_{SV} and γ_{LV} are measured in Joules per meter squared Jm^{-2}. Furthermore, γ_{SV} is measured in Newton per meter Nm^{-1}. Practically, liquid surface tension T and solid surface free energy SFE are measured in millinewton per meter mNm^{-1}. θ is the contact angle, as shown in Fig. 6 [109].

Table 6
The surface energy of some of the most used polymers as a substrate.

Material	SFE mNm^{-1}
PET polyethylene terephthalate	44.60
PVC polyvinyl chloride	41.50
PVF Polyvinyl fluoride	36.70
PE Polyethylene	35.70
LDPE	31
HDPE	31
PVDF Polyvinylidene fluoride	30.30
PP Polypropylene	30.10
OPP	29
PTFE Polytetrafluoroethylene	20
PDMS polydimethylsiloxane	19.80

The printability of the substrate mainly depends on its wettability behavior. Wettability and adhesion are the most important requirements in the printing process. Wettability and adhesion are directly related to the contact angle θ [27]. From Eq. (13), the contact angle will be

$$\cos\theta = \frac{\gamma_{SV} - \gamma_{SL}}{\gamma_{LV}} \tag{14}$$

The numerator determines whether the solid is wettable or not. If the surface free energy of the solid γ_{SV} is greater than the liquid surface tension γ_{SL}, the surface is called wettable or hydrophilic; otherwise, it is called non-wettable or hydrophobic. The solid surface is hydrophilic if $\theta < 90^0$ and hydrophilic if $90^\circ < \theta < 180^\circ$. The ink spreads uniformly on the surface when printed on hydrophilic substrates, while it forms droplets if printed on hydrophobic surfaces. Examples of substrates with high surface energy are ceramics, and substrates with low surface energy are polymers.

Young's equation does not consider the surface roughness, porosity, existence of impurities, and functional groups on the surface. All these surface properties influence the wettability and printing quality as a consequence.

The wettability can be improved either by elevating the substrate surface energy or by reducing the surface tension of the ink. This improves not only the wettability but also the adhesion and printing quality in general. The greater the difference between the substrate's surface energy and surface tension, the better the ink will wet and adhere to the substrate [115]. Paper substrates have excellent wettability. Textile printing issues were discussed shortly in Section 4.3, and polymer substrates usually have wettability issues because of their low surface energy. Table 6 presents the surface energy of some polymers; the surface energy values have been taken from [115] and DataPhysics Instruments company–a provider of measurement equipment for surface and interfacial science. The wettability of polymer substrates can be improved by cleaning the substrate surface and increasing its free energy. The purpose of cleansing is to eliminate contaminations like hydrocarbon oils, unwanted particles such as dust gathered by a static charge on the surface, or other chemicals used to fabricate the substrates [116]. The surface energy is mainly increased by generating more functional groups on the surface [115]. There are different techniques to increase the energy of the polymer surface, including coating the substrate with a wetting agent [117–119], mechanical roughening, chemical exposure and etching, corona, flame, and plasma treatment [120]. The advantage of mechanical roughening is its durability, with no deterioration or aging over time. The downside of chemical exposure is that the method has multiple processing steps (washing, rinsing, and drying) and generates a large amount of hazardous waste. Corona is the most widely used treatment method for polymer substrate surfaces [115].

Two important ink components affect surface tension: solvents and surfactants. Solvent-based inks have fewer wetting problems than water-based inks because solvents have a much lower surface tension than water, as shown in Table 7. Water-based inks require adding specific solvents and surfactants to reduce their surface tension. Typically, Alcohol solvents are more soluble in water than other solvents, and their surface tension is low. Due to this, they are usually added to water-based inks to reduce their surface tension. For instance, the surface energy of water has been reduced from 72 to 33 mNm^{-1} by adding ethanol. Solvent-based inks typically have surface tensions ranging from 20 to 30 mNm^{-1}, while water-based inks often have surface tensions ranging from 35 to 38 mNm^{-1} [115]. The boiling point BP of solvents determines their evaporation rate at sintering and storage temperature. The solvent should be volatile enough to evaporate quickly during sintering, but it should not be very volatile to avoid dryness on the ink in printers or shelves.

Due to the high volatility of solvents, they quickly spread in the air. Most of them are hazardous to human health and the environment, even causing ozone layer depletion [121]. The danger of solvents can be reduced by selecting a safer solvent; for instance, toluene and xylenes are alternatives to benzene — the more hazardous solvent. Some companies leading the pharmaceutical industry, such as Pfizer, Sanofi, and AstraZeneca, have classified solvents into three groups according to their hazardous level: preferred, usable, undesirable, or banned [122]. Table 7 presents the most used solvents in conductive ink formation, and all are classified as preferred or usable. Examples of undesirable solvents are benzene, hexanes, and halogenated hydrocarbons such as chloroform and methyl chloride [123].

Tag antennas are commonly printed on three substrates: papers, polymers and textiles. The applications determine which type is selected. Common problems with substrates include wettability, porosity, surface roughness and temperature sensitivity.

5. Printing techniques

Printing techniques have attracted researchers for the last two decades as an additive fabrication method. It has many advantages over etching techniques used in the semiconductor industry. It enables low material waste, is environment-friendly by using less hazardous chemicals, and is a user-friendly and low-cost fabrication process. Furthermore, its low temperature and suitability for large-area electronics made it suitable for fabricating flexible electronics in various fields, such as flexible screens, solar cells, sensors and RFID. The printing techniques most commonly used in research are inkjet and screen printing. In the following sections, they are discussed, and their printing parameters are related to the print quality and, therefore, the antenna efficiency.

5.1. Inkjet printing

Inkjet printing IJP is a non-contact deposition method used to deposit chemical materials on rigid or flexible substrates. Inkjet printing is preferred for its capability of automated production and provides patterns with high resolution. Moreover, inkjet printing is suitable for producing printed large-area electronics on flexible substrates [37]. There are two types of inkjet printers: the continuous inkjet printer CIJ and the drop-on-demand printer DOP. The continuous inkjet printer CIJ was invented first, and because of its complexity, it is not usually used for printing functional inks. Later, DOD printers were invented as an alternative to CIJ. The most used DOD printers are based on thermal and piezoelectric effects. Thermal head printers have lower costs than piezoelectric printers, but the latter can deposit a wider variety of materials on various substrates. DOD inkjet printers have extended from photocopying regular inks on paper to using materials inkjet printers to deposition functional inks and biological fluids. The conductive ink and the reducer agent can be loaded in different cartridges. Then, the deposition of the materials is controlled by setting the color degree of the designed pattern. The chemicals can be printed simultaneously [124,125], or on separate runs [126].

Table 7
Some of the frequently used solvents and some of their properties.

Solvent	CAS	BP °C	T [mNm^{-1}]	Solubility in water	Classification	Selection guide (Pfizer)
Water	7732-18-5	100	72.80	–	–	Preferred
Ethylene glycol	107-21-1	197.5	47.70	Miscible	Ether	Usable
Water : ethanol	–	–	33	–	–	–
o-Xylene	95-47-6	144.4	30.10	Insoluble	Hydrocarbon	Usable
m-Xylene	108-38-3	139.1	38.90	Insoluble	Hydrocarbon	Usable
Toluene	108-88-3	110.6	28.40	Insoluble	Hydrocarbon	Usable
n-butanol	71-36-3	117.7	25	Soluble	Alcohol	Preferred
1-Propanol	71-23-8	97.04	23.70	Miscible	Alcohol	Preferred
Ethyl acetate	141-78-6	77.10	23.60	Soluble	Ether	Preferred
Isopropanol	67-63-0	82.21	23	Miscible	Alcohol	Preferred
Methanol	64-17-5	78.24	22.10	Miscible	Alcohol	Preferred
N-Octane	111-65-9	125.62	21.62	Insoluble	Hydrocarbon	Unclassified

The boiling point, solubility in water, and classification of solvents were taken from [121]. A selection guide of solvents by Pfizer from [123]. Moreover, [99] compares several selection guides by different companies: Pfizer, GlaxoSmithKline, AstraZeneca, Sanofi, GCI-PR, and CHEM21. All companies gave quite similar assessments to those of Pfizer.

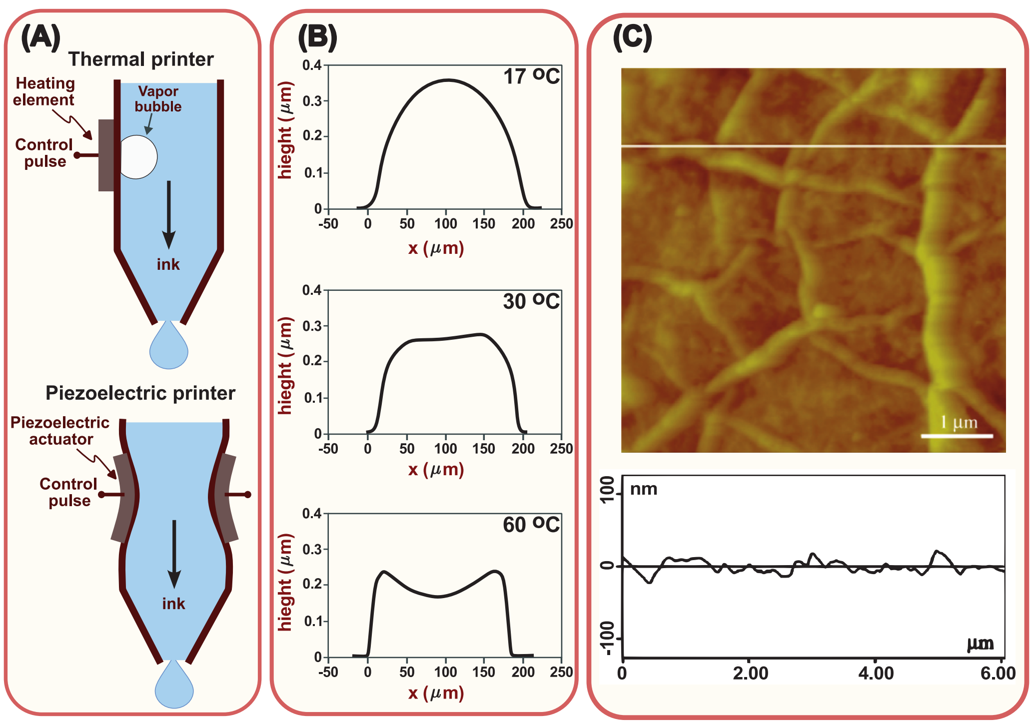

Fig. 7. (a) Schematic diagram of thermal and piezoelectric printers shows the mechanism of droplet generation. (b) Cross-section of printed single drops at three sintering temperatures shows the development of the coffee-ring effect. Reproduced with permission [119], 2008, American Chemical Society (C) Surface morphology of sintered graphene ink printed on the PI substrate and its roughness profile. Reproduced with permission [117], 2011, Springer.

Depending on how the ink is pushed out of the printhead to create the droplets, there are four types of DoD IJPs: thermal, piezoelectric, electrostatic and acoustic. Fig. 7(a) shows the head of thermal and piezo printers, the most commonly used printer types. Thermal printers use a resistance heating element to quickly heat the ink so that it evaporates and creates a bubble that pushes the ink out and forms a drop. Although thermal printers are the cheapest, they are not suitable for temperature-sensitive inks such as polymer inks because high temperatures can damage the ink. Piezoelectric printers use piezoelectric phenomena to deform the head to squeeze the ink and form droplets. There are no restrictions regarding the type of ink. Piezoelectric printers do not limit the use of ink type. They are a good choice for printing heat-sensitive inks and biomaterials. Most available material printers are piezoelectric, but their high cost is still a major disadvantage of this type of printer. Electrostatic printers use electrostatic force to eject the droplets. Although they offer higher resolution compared to piezoelectric printers, few manufacturers supply this type. In acoustic printers, the droplets are created by an ultrasonic beam generated by a piezoelectric element and focused by an acoustic lens. The head of this printer is safe from nozzle clogging, and they are applied for adhesive coatings [30].

The printability of the ink can be described by a dimensionless number Z, which is a function of the nozzle diameter (the diameter of the printing orifice) a and the physical parameters of the inks: viscosity η, density ρ, and surface tension γ. Z is defined by Eq. (15) [30,127]. The printable range is defined as $4 \geq Z \geq 14$ [127]. The droplet size increases as Z increases [128].

$$Z = \frac{(a\rho\gamma)^{\frac{1}{2}}}{\eta} \tag{15}$$

The problem with inkjet printing is the need to print multiple times to achieve the targeted thickness of the printed layer. Moreover, errors grow with the increased number of printing runs caused by ink spreading. [129]. Another common problem with inkjet-printed patterns is the coffee-ring effect, as reported by [119] for inkjet-printed conductive polymer ink (Fig. 7(b)) and by [117] for graphene-based

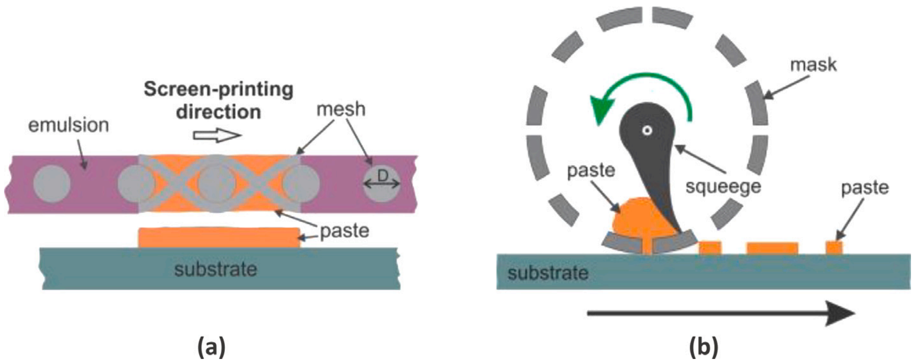

Fig. 8. Screen printing mesh. (a) Cross-section of the screen mesh. (b) Rotary screen printing system.
Source: Reproduced with permission [31], 2021, Elsevier.

inks (Fig. 7(c)) and by [129] for inkjet-printed silver ink. The coffee ring phenomenon happens due to the evaporation of volatile ink solvents after printing drop droplets on a substrate. It leaves behind a ring-like solid along the edges due to the outward flow of ink during drying–capillary effect [130]. Various strategies have been developed to suppress the coffee-ring effect, and even there are approaches to exploit this phenomenon for some applications [131].

5.2. Screen printing

Screen printing is a contact printing method for applying a patterned layer to various substrates by forcing a suspension called screen printing paste through a screen onto the substrate. In the electronics industry, screen printing deposits patterned layers of functional materials on various substrates. The screen consists of a mesh coated with an emulsion, leaving open areas representing the pattern to be printed and stretched by a metallic frame Fig. 6(a). In the printing process, the screen is placed on top of the substrate, with a 0.5–1 mm spacing gap between the mesh and the substrate. Then, an amount of paste is placed on the mesh and pushed with a squeegee made of polyurethane rubber supported by metal. The paste passes through the open areas, leaving a patterned layer on the substrate. Rotary screen printing enables mass production. Instead of a flat screen, a cylindrical screen is used. The squeegee is fixed while the cylinder is rotated at the same speed as the substrate moves. The paste is placed inside the cylinder and continuously pushed via the mesh, as shown in Fig. 6(b).

The mesh wire is typically made from polyamide, polyester, or stainless steel. Polyamide and polyester mesh distort, leading to a relatively thin layer. Stainless steel meshes have thin, uniform wires with very low extension, leading to high-resolution printing. The low flexibility of stainless-steel screens makes them only suitable for printing on flat surfaces. Due to this, they are mainly used in the electronics industry [31].

The thickness of the wet-printed layer WT is estimated by

$$WT = (MT \times OA) + ET \tag{16}$$

where MT is the thickness of the mesh. Meanwhile, $OA = [1-(M\times D)]^2$ is the percentage of opening area, M is the mesh count, i.e., the number of wires per inch, and D is the diameter of the mesh wires in inches. ET equals 13 μm for most of the applications [31]. A mesh with a high ratio of mesh count M and wire diameter D provides a high-resolution print [132]. However, the minimum size of the mesh openings must be 3–5 times greater than the size of the particle in the paste [31]. The layer thickness can be achieved by screen printing, ranging from a few micrometers to about 30 μm. A thicker layer can be achieved by repeating the printing after drying and sintering the previous layer. The process can be repeated until the targeted thickness is reached. The fabrication of tags involving narrow conductive traces (less than 1 mm) is feasible by screen printing, unlike gravure printing and flexography, which have an issue with narrow traces [41,46]. Recently, printed lines of 35μm width have been applied in the industry [31]. While an average finger width of 26.2μm was reported under laboratory conditions [133].

The printability of the paste is influenced by its rheological properties: viscosity and thixotropy. The two properties are dependent on the shear rate. Viscosity is the ratio of the shear stress τ to the shear rate $d\gamma/dt$ that the paste experiences during printing. High viscosity means high paste resistance to flow and vice versa [31]. The flow behavior of the paste is unlike water or pure solvents that show a Newtonian flow behavior, in which the viscosity does not change with the shear rate. The paste shows pseudoplastic flow behavior under pressing by squeegee during printing. The viscosity decreases as the shear rate increases in this stage, as Fig. 9(a) depicts. After the release of the squeegee, the viscosity increases again over time; this flow behavior is called thixotropic, shown in Fig. 9(b). In a true thixotropy, the paste retains exactly its initial viscosity. The area between the two curves in Fig. 9(b) represents the hysteresis loop; a small area indicates rapid viscosity recovery, which is important for realizing high-resolution print [56,134].

The performance of screen-printed tag antennas is comparable with etched tags [41]. However, screen printing suffers from an inherent problem of the surface roughness of the printed pattern. Also, the screen-printed pattern needs a thicker layer than the inkjet-printed pattern due to the higher skin depth caused by lower conductivity [41,129].

5.3. Electroless plating

Electroless plating is a method for coating surfaces of substrates or objects with metals. The substrate is immersed in a bath, bearing the metal to be deposited. Unlike electroplating, electroless plating does not require DC current for the redox to occur. Electroless plating has advantages over electroplating. For instance, the capability of producing uniform layers, the ability of deposition on dielectric substrates, and better controllability over layer thickness [135]. Because electroless plating enables an easily controllable, highly conductive, uniform, and smooth, dense deposited layer, it can be applied to thin and thick film metallization. The most concerns in the electroplating process are the stability of the bath and its longevity, cost, safety issues, and the properties of the deposited layer, especially metal purity, conductivity, uniformity, smoothness, and adhesion to the substrate.

Electroless plating solves the problem of nozzle-clogging in the case of inkjet printing and oxidation issues of some metals and is suitable for printing on temperature-sensitive substrates. Due to its ability to produce nearly pure metal traces, this technique is currently superior for obtaining excellent electrical characteristics of printed traces [32]. It can also be used as a complementary process of other printing techniques to improve the surface morphology, increase the conductivity of the top region of the printed pattern, and reduce the surface roughness

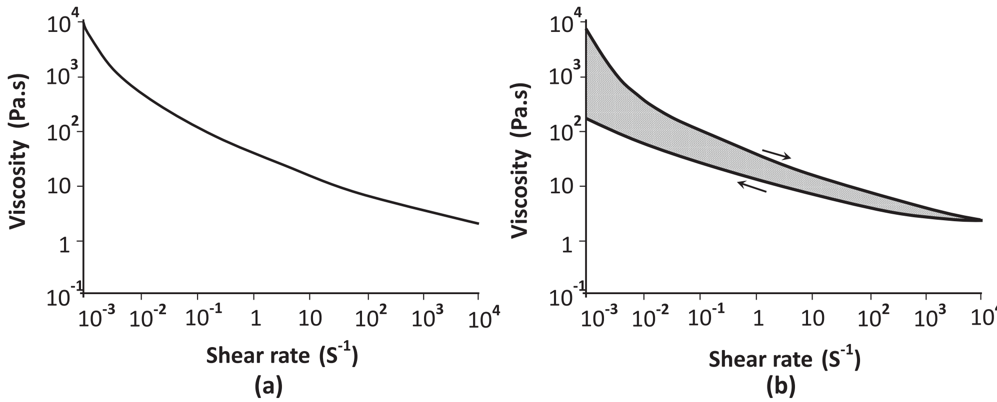

Fig. 9. The flow behavior of the screen printing paste. (a) Pseudoplastic flow behavior. (b) Thixotropic flow behavior.
Source: Reproduced with permission [56], 2010, John Wiley & Sons.

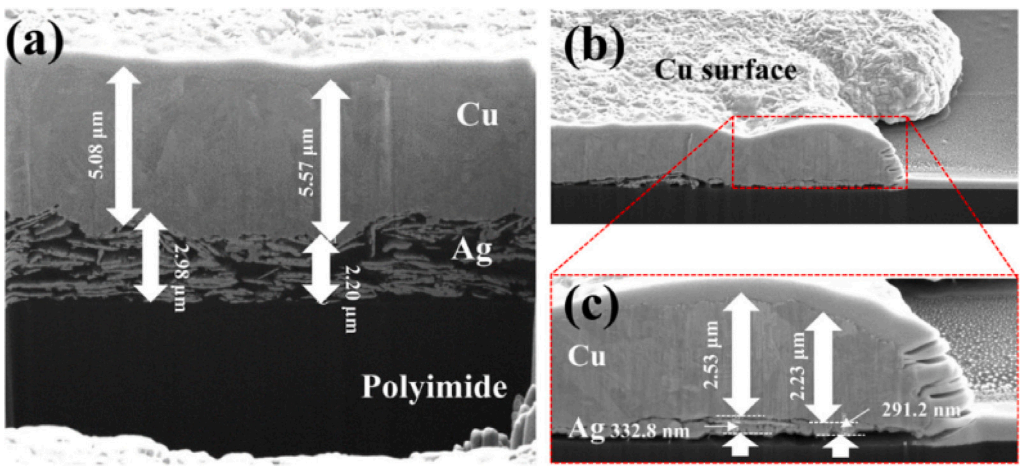

Fig. 10. Cross-section SEM images of Cu-plated layer on patterned Ag seed. (a) Ag pattern of about 3 µm thickness covered with 6 µm Cu layer. (b) A Cu layer plated at 60 °C for 50 min on an Ag seed of 300 nm thickness. (c) Zoomed-in view of (b).
Source: Reproduced with permission [34], 2015 Springer.

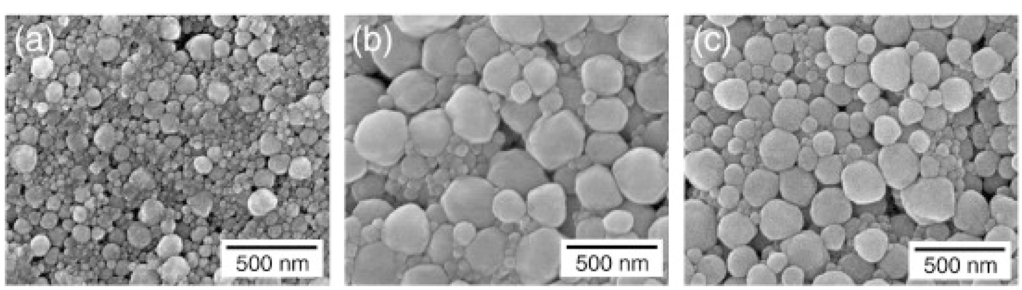

Fig. 11. Surface morphologies of copper films were obtained by sintering for 60 min at 110 °C (a), 140 °C (b), and 160 °C (c).
Source: Reproduced with permission [76], 2011, Elsevier.

commonly occurring, especially in screen printing. Fig. 10 depicts a cross-section of a printed layer; first, a silver screen was printed, and an electroless plating of copper was carried out. Fig. 8 shows that the plated copper layer is far smoother than the screen-printed silver layer. This method can improve the antenna performance as the most current flow near the surface. After the sintering and formation of metal nanoparticles, gaps between particles responsible for increasing the contact resistance between particles were observed on the surface, as shown in Fig. 11. Meanwhile, the particles were well connected at the bottom near the substrate [76].

The plating bath contains several constituents: metal salt, reducing agent, complexing agent, pH adjusting agent, and additives. The main components are metal salt and a reducing agent. The metal salts commonly used for electroless plating are silver nitride $AgNO_3$, copper sulfate $CuSO_4 \cdot 5\,H_2O$, nickel sulfate $NiSO_4 \cdot 6\,H_2O$, and nickel chloride, $NiCl_2 \cdot 6\,H_2O$. Reducers are added to react with the salt and produce a pure metal that deposits on the substrate surface with a catalytic ability. Complexing agents are added to increase the plating rate and enhance the bath stability. Two types of baths exist in terms of pH value: acid baths and alkaline baths. pH agents are responsible for maintaining the pH value at the level where the redox reaction works appropriately and controlling the plating rate. The pH level has an impact on the surface roughness and the crystallinity of the coating. The additives are added

Table 8
Comparison of electroless plating work using different seeds, plating bath, and plating conditions.

Seed	Printing method	Substrate	Coating	Salt	Reducer	Plating time, temp.	h[a] μm	Plating rate[b] nm/ min	ρ[c] μΩ cm	Ref.
Cu MOD	Inkjet	FR-4, filter paper	Copper	Copper salt [d]	CHOH[e]	45 °C	NA	NA	2.38	[32]
Ag NP	Screen	PI	Copper	NA	CHOH	60 °C, 50 min	3	60	NA	[34]
Pd NP	Inkjet	slag fiber paper	Copper	$CuSO_4$	CHOH	35 °C, 10 min	1.1	110	3.7	[136]
$PdCl_2$	Inkjet	Teslin paper	Copper	$CuSO_4$	CHOH	25 °C, 50 min	3.87	77.4	29.41	[137]
$AgNO_3$	Inkjet	A4 paper	Copper	$CuSO_4 \cdot 5H_2O$	CHOH	60 °C, 8 min	1.8	225	4500	[124]
$AgNO_3$	flexo.	paper	Copper	$CuSO_4 \cdot 5H_2O$	CHOH	45 °C, 25 min	2.41	96.4	2.22	[33]
$CuSO_4 \cdot 5H_2O$	Inkjet	PI	Copper	$CuSO_4 \cdot 5H_2O$	CHOH	60 °C, 30 min	14.3	408.5	5.68	[138]
$AgNO_3$	Inkjet	PET, PI	Copper	$CuSO_4 \cdot 5H_2O$	$C_2H_2O_2$	55 °C, 2 min	0.3	150	2.08	[35]
Cu NP	Inkjet	PET	Copper	$CuSO_4 \cdot 6H_2O$	DMAB	25 °C, 6 h	1	2.77	5.43	[139]
$AgNO_3$	different methods	various materials	Copper	$CuSO_4 \cdot 5H_2O$	CHOH[e]	NA	5	NA	1.85	[140]
Copper MOD	Screen	spandex	Copper	Copper salt [d]	CHOH[e]	60 min	≈ 2	33.33	10.29	[141]
$CuSO_4 \cdot 5H_2O$	Inkjet	Aluminum nitride	Copper	$CuSO_4 \cdot 6H_2O$	DMAB NaH_2PO_2	8 h	3	6.25	8.70	[142]
Pd NP	Inkjet	slag fiber paper	Nickel	$NiSO_4 \cdot 6H_2O$	$NaH_2PO \cdot H_2O$	75 °C, 10 min	2	200	76.1	[136]
$AgNO_3$	Screen	PET fabric	Silver	$AgNO_3$	Glucose	25 °C, 30 min	0.94	31.3	80.84	[143]

[a] h is the printed layer thickness.
[b] The plating rate was computed from the given data.
[c] ρ is the electrical resistivity.
[d] Commercial solution containing copper salt.
[e] Commercial solution containing Formaldehyde CHOH.

to stabilize the bath to increase its life by preventing decomposition from occurring [144].

The traditional copper plating baths are based on formaldehyde as a reducing agent [32–34,124,136–138]. These baths have two disadvantages. Firstly, formaldehyde baths require a high pH value of more than 11, limiting the number of substrates that can be used. Secondly, formaldehyde is a volatile colorless gas that is flammable, extremely toxic, and hazardous to human health [145].

Some researchers started to use safer alternatives to aldehydes reducers, e.g., glyoxal $C_2H_2O_2$ [35]. Dimethylamino borane DMAB has recently been used as a safer reducer than hazardous formaldehyde [139,142]. DMAB is a mild reducer, soluble in water, and operates in a wide range of pH values. DMAB bath provides a highly pure and smooth surface coating, has good stability, and does not decompose for six months [139]. Researchers have paid more attention to electroless plating of copper [146,147]. Sodium hypophosphite NaH_2PO_2 is the most attractive reducing agent due to its excellent bath stability, long life, safety, and it can be recycled [139]. Sodium hypophosphite is often used as a reducing agent for nickel salts. The possible pH value of the bath is in the range of 4–11. However, plating at low pH values (acidic range) will increase the phosphorous content in the deposited layer—up to 25% of phosphorous content results from plating at pH 4. Meanwhile, plating in the alkaline range yields less than 1% phosphorous content. Other reducing agents used for nickel plating along with their working pH range are sodium borohydride $NaBH_4$ (12–14 pH), dimethylamine borane DMAB $(CH_3)_2NHBH_3$ (6–10 pH), hydrazine $N_2H_4{\cdot}H_2O$ (8–11 pH). The reducing agents used for silver nitrate are Rochelle salt, glucose, and Hydrazine sulfate [144].

Table 8 presents details of selected works of electroless plating of Cu, Ni, and Ag, which are the metals used for plating. It is noticeable that formaldehyde is still mostly used as a reducing agent for copper salt. The lowest copper plating resistivity values obtained by using formaldehyde as the reducing agent are 1.85 μΩ cm [140], 2.22 μΩ cm [33] and 2.38 μΩ cm [32]. These values are comparable to the resistivity of bulk copper (1.68 μΩ cm). A lower resistivity of 2.08μΩ cm was achieved at a higher deposition rate using glyoxal as the reducing agent instead of formaldehyde [35]. Although glyoxal is an aldehyde compound, it is less toxic than formaldehyde. In [139,142], DMAB was the reducing agent, and the resistivity values were 5.43 and 8.7 μΩ cm, respectively. However, the deposition rate is slow, as can be seen in Table 8 and as reported by [142]. Two high resistivity values of 29.41 and 4500 μΩ cm made of deposited copper [124,137] and another of 67.1 μΩ cm made of deposited nickel are all printed on various paper substrates [136], the resistivity increased as the substrate roughness increased. A similar scenario happened for deposited copper on spandex textile [141] and silver on PET fabric [143].

The electroless plating method is used for the synthesis of core–shell nanoparticles. Typically, Cu NPs (copper powder) are coated by silver [148,149], or Ni NPs are coated by silver [72]; the silver precursor is silver nitrate. Before the plating, the oxide layer must be removed to allow silver to deposit on the surface of core particles, yielding a high-quality core–shell composite powder. The synthesis of the core–shell nanoparticle can be driven by a transmetalation reaction, in which the copper atoms on the surface of the particles act as a reducing agent for the silver. Using this method, the coating is uniform and solely Cu-Ag core–shell NPs, with no individual silver particles formed [69].

The most commonly used techniques for printing tag antennas are inkjet printing and screen printing. Inkjet printing provides high-resolution prints, but multiple prints are required to achieve the desired thickness, reducing printing accuracy and the coffee ring effect, which is a common problem. Screen printing uses ink with a higher viscosity than inkjet printers, which produce a thicker layer because they contain more conductive materials. Screen printed patterns are uneven, which negatively affects UHF components, especially antennas. Electroless plating is used as a complementary process to correct defects in patterns printed by inkjet or screen printing, or a seed layer is printed using one of these methods and then electroless plated to produce dense, smooth, and highly conductive patterns.

6. Conclusion

The efficiency of the RFID tag antenna is highly dependent on its electrical conductivity, thickness, and surface morphology. There are different types of ink: metal NP ink, metal particle-free ink, polymer-based ink, and carbon-based ink. When long-distance communication is required, particle-free ink is a good choice. In addition, this type of ink is easier to prepare, more stable, has a longer shelf life and better electrical properties, and solves nozzle clogging that often occurs when printing nanoparticle inks. Therefore, metal particle-free ink is a potential replacement for metal nanoparticle ink for flexible electronics, especially flexible antennas. The formation of organometallic decomposition MOD inks using metal complexes offers several advantages over metal salt inks. MOD ink lowers the decomposition temperature and can produce a nearly pure, highly conductive layer by reducing organic residue.

Additionally, MOD inks are more stable. Polymer-based ink is the most suitable choice for wearable applications due to its high flexibility and stretchability, but this advantage comes with the cost of communication distance. Carbon-based ink is becoming increasingly popular due to its low cost and environmental friendliness. Three different types of substrates are primarily used for flexible electronics, with the choice depending on the application. Several challenges are often encountered when printing these substrates, including wettability, porosity, surface roughness, and temperature sensitivity. Several methods to overcome these challenges include coating, treating the substrate surface to improve wettability, and customizing the ink using appropriate additives and solvents to improve wettability and adhesion to the substrate. Printing as an additive manufacturing method is preferred over subtractive methods for flexible electronics. There are different printing methods, and each method has its advantages, disadvantages, and limitations. Inkjet printing and screen printing outperform other printing techniques. Inkjet printing is commonly used for particle-free inks, whereas nanoparticle inks are commonly produced using screen printing. Both can be used in the laboratory or automated for mass production. Finally, the electroless plating offers excellent electrical properties compared to other printing processes and enables printing quickly oxidizable metals, e.g., copper, at low temperatures. In addition, it is a method that allows the synthesis of core–shell nanoparticles.

CRediT authorship contribution statement

Mohd Nizar Hamidon: Validation, Supervision, Methodology, Funding acquisition, Conceptualization. **Tark D. Farnana:** Writing – review & editing, Writing – original draft, Visualization, Software, Methodology, Investigation, Formal analysis, Data curation, Conceptualization. **Intan H. Hasan:** Writing – review & editing, Validation, Resources, Funding acquisition, Conceptualization. **Aduwati Sali:** Writing – review & editing, Validation, Supervision, Resources. **Maryam Md. Isa:** Validation, Resources, Project administration, Investigation.

Declaration of competing interest

The authors declare that they have no known competing financial interests or personal relationships that could have appeared to influence the work reported in this paper.

References

[1] F. Thiesse, T. Staake, P. Schmitt, E. Fleisch, The rise of the "next-generation bar code": an international RFID adoption study, Supply Chain Manag. Int. J. 16 (5) (2011) 328–345, http://dx.doi.org/10.1108/13598541111155848.

[2] R. Ramanathan, U. Ramanathan, L.W.L. Ko, Adoption of RFID technologies in UK logistics: Moderating roles of size, barcode experience and government support, Expert Syst. Appl. 41 (1) (2014) 230–236, http://dx.doi.org/10.1016/j.eswa.2013.07.024.

[3] A. Akbari, S. Mirshahi, M. Hashemipour, Comparison of RFID system and barcode reader for manufacturing processes, in: 2015 IEEE 28th Canadian Conference on Electrical and Computer Engineering, CCECE, IEEE, 2015, pp. 502–506, http://dx.doi.org/10.1109/CCECE.2015.7129326.

[4] E.M. Amin, N. Karmakar, S. Preradovic, Towards an intelligent EM barcode, in: 2012 7th International Conference on Electrical and Computer Engineering, IEEE, 2012, pp. 826–829, http://dx.doi.org/10.1109/ICECE.2012.6471678.

[5] E. Pereira, Í. Araújo, L.F.V. Silva, M. Batista, S. Júnior, E. Barboza, E. Santos, F. Gomes, I.T. Fraga, R. Davanso, et al., RFID technology for animal tracking: A survey, IEEE J. Radio Frequency Identif. 7 (2023) 609–620, http://dx.doi.org/10.1109/JRFID.2023.3334952.

[6] J. Xu, Z. Li, K. Zhang, J. Yang, N. Gao, Z. Zhang, Z. Meng, The principle, methods and recent progress in RFID positioning techniques: A review, IEEE J. Radio Frequency Identif. 7 (2023) 50–63, http://dx.doi.org/10.1109/JRFID.2022.3233855.

[7] Y. Qiu, J. Chen, Q. Zhu, Campus access control system based on RFID, in: 2012 IEEE International Conference on Computer Science and Automation Engineering, IEEE, 2012, pp. 407–410, http://dx.doi.org/10.1109/ICSESS.2012.6269491.

[8] M. Siva ganga prasad, D. Pranitha, V. Chakra rao, V. Pavankumar, G. Sandeep, Automated toll plaza using RFID, in: ICCCE 2021: Proceedings of the 4th International Conference on Communications and Cyber Physical Engineering, Springer, 2022, pp. 1091–1103, http://dx.doi.org/10.1007/978-981-16-7985-8_114.

[9] V. Mulloni, M. Donelli, Chipless RFID sensors for the internet of things: Challenges and opportunities, Sensors 20 (7) (2020) 2135, http://dx.doi.org/10.3390/s20072135.

[10] A. Sharif, Q.H. Abbasi, K. Arshad, S. Ansari, M.Z. Ali, J. Kaur, H.T. Abbas, M.A. Imran, Machine learning enabled food contamination detection using RFID and internet of things system, J. Sensor Actuator Netw. 10 (4) (2021) 63, http://dx.doi.org/10.3390/jsan10040063.

[11] A. Ahmadihaji, R. Izquierdo, A. Shih, From chip-based to chipless RFID sensors: a review, IEEE Sensors J. (2023) http://dx.doi.org/10.1109/JSEN.2023.3266316.

[12] A.W. Nagpurkar, S.K. Jaiswal, An overview of WSN and RFID network integration, in: 2015 2nd International Conference on Electronics and Communication Systems, ICECS, IEEE, 2015, pp. 497–502, http://dx.doi.org/10.1109/ECS.2015.7124956.

[13] L. Mainetti, L. Palano, L. Patrono, M.L. Stefanizzi, R. Vergallo, Integration of RFID and WSN technologies in a smart parking system, in: 2014 22nd International Conference on Software, Telecommunications and Computer Networks, SoftCOM, IEEE, 2014, pp. 104–110, http://dx.doi.org/10.1109/SOFTCOM.2014.7039099.

[14] X. Xiao, B. Mu, G. Cao, Y. Yang, M. Wang, Flexible battery-free wireless electronic system for food monitoring, J. Sci. Adv. Mater. Devices 7 (2) (2022) 100430, http://dx.doi.org/10.1016/j.jsamd.2022.100430.

[15] C. Yue, J. Wang, Z. Wang, B. Kong, G. Wang, Flexible printed electronics and their applications in food quality monitoring and intelligent food packaging: Recent advances, Food Control (2023) 109983, http://dx.doi.org/10.1016/j.foodcont.2023.109983.

[16] A. Mostaccio, G.M. Bianco, G. Marrocco, C. Occhiuzzi, RFID technology for food industry 4.0: A review of solutions and applications, IEEE J. Radio Frequency Identif. (2023) http://dx.doi.org/10.1109/JRFID.2023.3278722.

[17] S.I. Khan, B.R. Ray, N.C. Karmakar, RFID localization in construction with iot and security integration, Autom. Constr. 159 (2024) 105249, http://dx.doi.org/10.1016/j.autcon.2023.105249.

[18] K.-K. Duan, S.-Y. Cao, Emerging RFID technology in structural engineering–a review, in: Structures, Vol. 28, Elsevier, 2020, pp. 2404–2414, http://dx.doi.org/10.1016/j.istruc.2020.10.036.

[19] L. Catarinucci, D. De Donno, L. Mainetti, L. Palano, L. Patrono, M.L. Stefanizzi, L. Tarricone, Integration of UHF RFID and WSN technologies in healthcare systems, in: 2014 IEEE RFID Technology and Applications Conference (RFID-TA), IEEE, 2014, pp. 289–294, http://dx.doi.org/10.1109/RFID-TA.2014.6934245.

[20] Q. Tao, S. Liu, J. Zhang, J. Jiang, Z. Jin, Y. Huang, X. Liu, S. Lin, X. Zeng, X. Li, et al., Clinical applications of smart wearable sensors, Iscience 26 (9) (2023) http://dx.doi.org/10.1016/j.isci.2023.107485.

[21] S.G. Kirtania, A.W. Elger, M.R. Hasan, A. Wisniewska, K. Sekhar, T. Karacolak, P.K. Sekhar, Flexible antennas: A review, Micromachines 11 (9) (2020) 847, http://dx.doi.org/10.3390/mi11090847.

[22] A. Kiourti, J.L. Volakis, Wearable Antennas and Electronics, Artech House, 2022.

[23] P. Martins, N. Pereira, A. Lima, A. Garcia, C. Mendes-Filipe, R. Policia, V. Correia, S. Lanceros-Mendez, Advances in printing and electronics: From engagement to commitment, Adv. Funct. Mater. 33 (16) (2023) 2213744, http://dx.doi.org/10.1002/adfm.202213744.

[24] M. Dulal, S. Afroj, J. Ahn, Y. Cho, C. Carr, I.-D. Kim, N. Karim, Toward sustainable wearable electronic textiles, ACS Nano 16 (12) (2022) 19755–19788, http://dx.doi.org/10.1021/acsnano.2c07723.

[25] J. Wiklund, A. Karakoç, T. Palko, H. Yiğitler, K. Ruttik, R. Jäntti, J. Paltakari, A review on printed electronics: fabrication methods, inks, substrates, applications and environmental impacts, J. Manuf. Mater. Process. 5 (3) (2021) 89, http://dx.doi.org/10.3390/jmmp5030089.

[26] Y. Htwe, M. Mariatti, Printed graphene and hybrid conductive inks for flexible, stretchable, and wearable electronics: Progress, opportunities, and challenges, J. Sci. Adv. Mater. Devices 7 (2) (2022) 100435, http://dx.doi.org/10.1016/j.jsamd.2022.100435.

[27] S.M.F. Cruz, L.A. Rocha, J.C. Viana, Printing technologies on flexible substrates for printed electronics, in: Flexible Electronics, IntechOpen, 2018, http://dx.doi.org/10.5772/intechopen.76161.

[28] W. Yang, X. Cheng, Z. Guo, Q. Sun, J. Wang, C. Wang, Design, fabrication and applications of flexible RFID antennas based on printed electronic materials and technologies, J. Mater. Chem. C 11 (2023) 406–425, http://dx.doi.org/10.1039/D2TC03736J.

[29] V. Beedasy, P.J. Smith, Printed electronics as prepared by inkjet printing, Materials 13 (3) (2020) 704, http://dx.doi.org/10.3390/ma13030704.

[30] A. Soleimani-Gorgani, Inkjet printing, in: Printing on Polymers, Elsevier, 2016, pp. 231–246, http://dx.doi.org/10.1016/B978-0-323-37468-2.00014-2.

[31] D. Kuscer, Screen printing, Elsevier, 2021, http://dx.doi.org/10.1016/B978-0-12-803581-8.12082-X.

[32] K. Chew, Y. Farraj, S. Magdassi, Electroless plating with copper complex ink as a seed, in: 2020 IEEE 22nd Electronics Packaging Technology Conference, EPTC, IEEE, 2020, pp. 36–40, http://dx.doi.org/10.1109/EPTC50525.2020.9315010.

[33] Y. Wang, Y. Huang, Y.-z. Li, P. Cheng, S.-y. Cheng, Q. Liang, Z.-q. Xu, H.-j. Chen, Z.-s. Feng, A facile process combined with roll-to-roll flexographic printing and electroless deposition to fabricate RFID tag antenna on paper substrates, Composites B 224 (2021) 109194, http://dx.doi.org/10.1016/j.compositesb.2021.109194.

[34] E.K. Choi, J. Park, B.S. Kim, D. Lee, Fabrication of electrodes and near-field communication tags based on screen printing of silver seed patterns and copper electroless plating, Int. J. Precis. Eng. Manuf. 16 (2015) 2199–2204, http://dx.doi.org/10.1007/s12541-015-0283-y.

[35] Y.-C. Liao, Z.-K. Kao, Direct writing patterns for electroless plated copper thin film on plastic substrates, ACS Appl. Mater. Interfaces 4 (10) (2012) 5109–5113, http://dx.doi.org/10.1021/am301654j.

[36] A. Hussain, H.L. Lee, S.J. Moon, Sintering of silver nanoparticle structures and the pursuit of minimum resistivity, Mater. Today Commun. 34 (2023) 105159, http://dx.doi.org/10.1016/j.mtcomm.2022.105159.

[37] A. Kamyshny, S. Magdassi, Conductive nanomaterials for printed electronics, Small 10 (17) (2014) 3515–3535, http://dx.doi.org/10.1002/smll.201303000.

[38] K.S. Rao, P.V. Nikitin, S.F. Lam, Antenna design for UHF RFID tags: A review and a practical application, IEEE Trans. Antennas Propagat. 53 (12) (2005) 3870–3876, http://dx.doi.org/10.1109/TAP.2005.859919.

[39] K. Rao, P. Nikitin, S. Lam, Impedance matching concepts in RFID transponder design, in: Fourth IEEE Workshop on Automatic Identification Advanced Technologies, AutoID'05, 2005, pp. 39–42, http://dx.doi.org/10.1109/AUTOID.2005.35.

[40] L. Catarinucci, D. De Donno, R. Colella, F. Ricciato, L. Tarricone, A cost-effective SDR platform for performance characterization of RFID tags, IEEE Trans. Instrum. Meas. 61 (4) (2012) 903–911, http://dx.doi.org/10.1109/TIM.2011.2174899.

[41] T. Björninen, S. Merilampi, L. Ukkonen, L. Sydänheimo, P. Ruuskanen, et al., The effect of fabrication method on passive UHF RFID tag performance, Int. J. Antennas Propagat. 2009 (2009) 1–8, http://dx.doi.org/10.1155/2009/920947.

[42] M. Shahpari, D.V. Thiel, The impact of reduced conductivity on the performance of wire antennas, IEEE Trans. Antennas and Propagation 63 (11) (2015) 4686–4692, http://dx.doi.org/10.1109/TAP.2015.2479241.

[43] P.V. Nikitin, S. Lam, K. Rao, Low cost silver ink RFID tag antennas, in: 2005 IEEE Antennas and Propagation Society International Symposium, Vol. 2, IEEE, 2005, pp. 353–356, http://dx.doi.org/10.1109/APS.2005.1552015.

[44] D. Deavours, K. Demarest, A. Syed, Effects of antenna material on the performance of UHF RFID tags, in: 2007 IEEE International Conference on RFID, IEEE, 2007, pp. 57–62, http://dx.doi.org/10.1109/RFID.2007.346150.

[45] P. Kopyt, B. Salski, M. Olszewska-Placha, D. Janczak, M. Sloma, T. Kurkus, M. Jakubowska, W. Gwarek, Graphene-based dipole antenna for a UHF RFID tag, IEEE Trans. Antennas and Propagation 64 (7) (2016) 2862–2868, http://dx.doi.org/10.1109/TAP.2016.2565696.

[46] S.L. Merilampi, T. Björninen, A. Vuorimäki, L. Ukkonen, P. Ruuskanen, L. Sydänheimo, The effect of conductive ink layer thickness on the functioning of printed UHF RFID antennas, Proc. IEEE 98 (9) (2010) 1610–1619, http://dx.doi.org/10.1109/JPROC.2010.2050570.

[47] J. Sidén, M. Fein, A. Koptyug, H.-E. Nilsson, Printed antennas with variable conductive ink layer thickness, IET Microw. Antennas Propag. 1 (2) (2007) 401–407, http://dx.doi.org/10.1049/iet-map:20060021.

[48] T. Thomas, Characterization of surface roughness, Precis. Eng. 3 (2) (1981) 97–104, http://dx.doi.org/10.1016/0141-6359(81)90043-X.

[49] P. Sahoo, Surface topography, in: Tribology for Engineers, Elsevier, 2011, pp. 1–32, http://dx.doi.org/10.1533/9780857091444.1.

[50] R.M. Morais, M.S. Klem, M.S. Ozório, T.C. Gomes, N. Alves, Roughness influence on the sheet resistance of the PEDOT: PSS printed on paper, Curr. Appl. Phys. 18 (2) (2018) 254–260, http://dx.doi.org/10.1016/j.cap.2017.11.008.

[51] A. Boumegnane, S. Douhi, A. Batine, T. Dormois, C. Cochrane, A. Nadi, O. Cherkaoui, M. Tahiri, Rheological properties and inkjet printability of a green silver-based conductive ink for wearable flexible textile antennas, Sensors 24 (9) (2024) 2938, http://dx.doi.org/10.3390/s24092938.

[52] C. Zheng, J. Hu, J. Jiang, Effect of fabric structure on the performance of screen-printed ultra-high frequency radio frequency identification tag antenna for wireless radio frequency energy harvesting, J. Ind. Textiles 52 (2022) 15280837221109641.

[53] B. Das, S. Mohanty, A comprehensive review on piezoelectric inks: From concept to application, Sensors Actuators A (2023) 114939, http://dx.doi.org/10.1016/j.sna.2023.114939.

[54] N. Ibrahim, J.O. Akindoyo, M. Mariatti, Recent development in silver-based ink for flexible electronics, J. Sci. Adv. Mater. Devices 7 (1) (2022) 100395, http://dx.doi.org/10.1016/j.jsamd.2021.09.002.

[55] Z. Żołek-Tryznowska, Additives for ink manufacture, in: Printing on Polymers, Elsevier, 2016, pp. 57–66, http://dx.doi.org/10.1016/B978-0-323-37468-2.00004-X.

[56] J. Bieleman, Additives for Coatings, Wiley-VCH, 2010.

[57] H.R. Tiyyagura, P. Majerič, Ž. Jelen, R. Rudolf, Gold nano-inks: synthesis and characterizations, in: Smart Multifunctional Nano-Inks, Elsevier, 2023, pp. 53–73, http://dx.doi.org/10.1016/B978-0-323-91145-0.00017-7.

[58] H.R. Tiyyagura, P. Majerič, M. Bračič, I. Anžel, R. Rudolf, Gold inks for inkjet printing on photo paper: Complementary characterisation, Nanomaterials 11 (3) (2021) 599, http://dx.doi.org/10.3390/nano11030599.

[59] A. Maattanen, P. Ihalainen, P. Pulkkinen, S. Wang, H. Tenhu, J. Peltonen, Inkjet-printed gold electrodes on paper: Characterization and functionalization, ACS Appl. Mater. Interfaces 4 (2) (2012) 955–964, http://dx.doi.org/10.1021/am201609w.

[60] P. Bishop, L. Ashfield, A. Berzins, A. Boardman, V. Buche, J. Cookson, R. Gordon, C. Salcianu, P. Sutton, Printed gold for electronic applications, Gold Bull. 43 (2010) 181–188, http://dx.doi.org/10.1007/BF03214985.

[61] H. Nur, J. Song, J. Evans, M. Edirisinghe, Ink-jet printing of gold conductive tracks, J. Mater. Sci., Mater. Electron. 13 (2002) 213–219, http://dx.doi.org/10.1023/A:1014827900606.

[62] X. Zeng, P. He, M. Hu, W. Zhao, H. Chen, L. Liu, J. Sun, J. Yang, Copper inks for printed electronics: a review, Nanoscale 14 (43) (2022) 16003–16032, http://dx.doi.org/10.1039/D2NR03990G.

[63] W. Li, Q. Sun, L. Li, J. Jiu, X.-Y. Liu, M. Kanehara, T. Minari, K. Suganuma, The rise of conductive copper inks: challenges and perspectives, Appl. Mater. Today 18 (2020) 100451, http://dx.doi.org/10.1016/j.apmt.2019.100451.

[64] P. Karthik, S.P. Singh, et al., Copper conductive inks: synthesis and utilization in flexible electronics, RSC Adv. 5 (79) (2015) 63985–64030, http://dx.doi.org/10.1039/C5RA08205F.

[65] H. Murthy, N. Thakur, N. Shankhwar, Nickel-based inks for flexible electronics—a review on recent trends, J. Adv. Manuf. Syst. 21 (03) (2022) 591–624, http://dx.doi.org/10.1142/S0219686722500214.

[66] N. Thakur, H. Murthy, Nickel-based inks for inkjet printing: a review on latest trends, Am. J. Mater. Sci. 11 (1) (2021) 20–35, http://dx.doi.org/10.5923/j.materials.20211101.03.

[67] Y. Lee, C.H. Kim, D.-Y. Shin, Y.G. Kim, Printed UHF RFID antennas with high efficiencies using nano-particle silver ink, J. Nanosci. Nanotechnol. 11 (7) (2011) 6425–6428, http://dx.doi.org/10.1166/jnn.2011.4390.

[68] J. Li, B. An, J. Qin, Y. Wu, Nano copper conductive ink for RFID application, in: 2011 International Symposium on Advanced Packaging Materials, APM, IEEE, 2011, pp. 91–93, http://dx.doi.org/10.1109/ISAPM.2011.6105678.

[69] M. Grouchko, A. Kamyshny, S. Magdassi, Formation of air-stable copper–silver core–shell nanoparticles for inkjet printing, J. Mater. Chem. 19 (19) (2009) 3057–3062, http://dx.doi.org/10.1039/b821327e.

[70] A. Pajor-Świerzy, R. Socha, R. Pawłowski, P. Warszyński, K. Szczepanowicz, Application of metallic inks based on nickel-silver core–shell nanoparticles for fabrication of conductive films, Nanotechnology 30 (22) (2019) 225301, http://dx.doi.org/10.1088/1361-6528/ab0467.

[71] A. Pajor-Świerzy, D. Gaweł, E. Drzymała, R. Socha, M. Parlińska-Wojtan, K. Szczepanowicz, P. Warszyński, The optimization of methods of synthesis of nickel–silver core–shell nanoparticles for conductive materials, Nanotechnology 30 (1) (2018) 015601, http://dx.doi.org/10.1088/1361-6528/aae677.

[72] J.J. Jing, J. Xie, G.Y. Chen, W.H. Li, M.M. Zhang, Preparation of nickel–silver core–shell nanoparticles by liquid-phase reduction for use in conductive paste, J. Exp. Nanosci. 10 (17) (2015) 1347–1356, http://dx.doi.org/10.1080/17458080.2015.1012751.

[73] W. Yang, E.J. List-Kratochvil, C. Wang, Metal particle-free inks for printed flexible electronics, J. Mater. Chem. C 7 (48) (2019) 15098–15117, http://dx.doi.org/10.1039/C9TC05463D.

[74] G. Cummins, M.P. Desmulliez, Inkjet printing of conductive materials: a review, Circuit World 38 (4) (2012) 193–213, http://dx.doi.org/10.1108/03056121211280413.

[75] S.P. Douglas, S. Mrig, C.E. Knapp, MODs vs. NPs: Vying for the future of printed electronics, Chem. Eur. J. 27 (31) (2021) 8062–8081, http://dx.doi.org/10.1002/chem.202004860.

[76] A. Yabuki, N. Arriffin, M. Yanase, Low-temperature synthesis of copper conductive film by thermal decomposition of copper–amine complexes, Thin Solid Films 519 (19) (2011) 6530–6533, http://dx.doi.org/10.1016/j.tsf.2011.04.112.
[77] W. Xu, T. Wang, Synergetic effect of blended alkylamines for copper complex ink to form conductive copper films, Langmuir 33 (1) (2017) 82–90, http://dx.doi.org/10.1021/acs.langmuir.6b03668.
[78] Y. Farraj, M. Grouchko, S. Magdassi, Self-reduction of a copper complex MOD ink for inkjet printing conductive patterns on plastics, Chem. Commun. 51 (9) (2015) 1587–1590, http://dx.doi.org/10.1039/C4CC08749F.
[79] L. Zhang, G. Gan, P. Fan, Y. Liu, T. Wang, W. Li, J. Du, Facile preparation of particle-free hybrid amine silver ink with synergistic effect for low-resistivity flexible films, J. Coatings Technol. Res. 20 (6) (2023) 1845–1856, http://dx.doi.org/10.1007/s11998-023-00781-8.
[80] W. Yang, Z. Dong, Z. Guo, H. Sun, Copper particle-free ink with enhanced performance for inkjet-printed flexible UWB antennas, J. Mater. Chem. C 11 (41) (2023) 14429–14438, http://dx.doi.org/10.1039/D3TC02515B.
[81] A. Yabuki, S. Kawahara, S. Kang, I.W. Fathona, Low-temperature synthesis of copper conductivity film from a copper formate amine complex with a low boiling point, Mater. Sci. Eng. B 262 (2020) 114743, http://dx.doi.org/10.1016/j.mseb.2020.114743.
[82] A.L. Dearden, P.J. Smith, D.-Y. Shin, N. Reis, B. Derby, P. O'Brien, A low curing temperature silver ink for use in ink-jet printing and subsequent production of conductive tracks, Macromol. Rapid Commun. 26 (4) (2005) 315–318, http://dx.doi.org/10.1002/marc.200400445.
[83] J.-T. Wu, S.L.-C. Hsu, M.-H. Tsai, W.-S. Hwang, Inkjet printing of low-temperature cured silver patterns by using $AgNO_3$/1-dimethylamino-2-propanol inks on polymer substrates, J. Phys. Chem. C 115 (22) (2011) 10940–10945, http://dx.doi.org/10.1021/jp200972y.
[84] S.B. Walker, J.A. Lewis, Reactive silver inks for patterning high-conductivity features at mild temperatures, J. Am. Chem. Soc. 134 (3) (2012) 1419–1421, http://dx.doi.org/10.1021/ja209267c.
[85] X. Nie, H. Wang, J. Zou, Inkjet printing of silver citrate conductive ink on PET substrate, Appl. Surf. Sci. 261 (2012) 554–560, http://dx.doi.org/10.1016/j.apsusc.2012.08.054.
[86] S.-P. Chen, Z.-K. Kao, J.-L. Lin, Y.-C. Liao, Silver conductive features on flexible substrates from a thermally accelerated chain reaction at low sintering temperatures, ACS Appl. Mater. Interfaces 4 (12) (2012) 7064–7068, http://dx.doi.org/10.1021/am302505j.
[87] Y. Dong, X. Li, S. Liu, Q. Zhu, J.-G. Li, X. Sun, Facile synthesis of high silver content MOD ink by using silver oxalate precursor for inkjet printing applications, Thin Solid Films 589 (2015) 381–387.
[88] K.S. Bhat, R. Ahmad, Y. Wang, Y.-B. Hahn, Low-temperature sintering of highly conductive silver ink for flexible electronics, J. Mater. Chem. C 4 (36) (2016) 8522–8527, http://dx.doi.org/10.1039/C6TC02751B.
[89] Y. Dong, X. Li, S. Liu, Q. Zhu, M. Zhang, J.-G. Li, X. Sun, Optimizing formulations of silver organic decomposition ink for producing highly-conductive features on flexible substrates: The case study of amines, Thin Solid Films 616 (2016) 635–642, http://dx.doi.org/10.1016/j.tsf.2016.09.024.
[90] M. Vaseem, G. McKerricher, A. Shamim, Robust design of a particle-free silver-organo-complex ink with high conductivity and inkjet stability for flexible electronics, ACS Appl. Mater. Interfaces 8 (1) (2016) 177–186, http://dx.doi.org/10.1021/acsami.5b08125.
[91] Y. Zhou, Z. Xu, H. Bai, C.E. Knapp, Room temperature electronic functionalization of thermally sensitive substrates by Inkjet printing of a reactive silver-based MOD ink, Adv. Mater. Technol. 8 (8) (2023) 2201557, http://dx.doi.org/10.1002/admt.202201557.
[92] M. Sun, C. Li, Y. Xu, B. Lin, X. Zhang, Y. Sun, An conductive ink based on silver oxide complex for low-temperature sintering with dense conductive paths, J. Mater. Sci., Mater. Electron. 35 (11) (2024) 755, http://dx.doi.org/10.1007/s10854-024-12524-5.
[93] T. Qi, Z. Zhang, Y. Li, J. Wang, F. Xiao, A low temperature self-reducible copper hydroxide amino–alcohol complex catalyzed by formic acid for conductive copper films, J. Mater. Chem. C 6 (42) (2018) 11320–11327, http://dx.doi.org/10.1039/C8TC02665C.
[94] Y. Dong, Z. Lin, X. Li, Q. Zhu, J.-G. Li, X. Sun, A low temperature and air-sinterable copper–diamine complex-based metal organic decomposition ink for printed electronics, J. Mater. Chem. C 6 (24) (2018) 6406–6415, http://dx.doi.org/10.1039/C8TC01849A.
[95] W. Yang, C. Wang, V. Arrighi, One step preparation of copper–silver self-catalyzed hybrid conductive ink with reduced sintering temperature for flexible electronics, J. Mater. Sci., Mater. Electron. 30 (2019) 11607–11618, http://dx.doi.org/10.1007/s10854-019-01518-3.
[96] W. Li, C.-F. Li, F. Lang, J. Jiu, M. Ueshima, H. Wang, Z.-Q. Liu, K. Suganuma, Self-catalyzed copper–silver complex inks for low-cost fabrication of highly oxidation-resistant and conductive copper–silver hybrid tracks at a low temperature below 100°C, Nanoscale 10 (11) (2018) 5254–5263, http://dx.doi.org/10.1039/C7NR09225C.
[97] J. Lundquist, L. Linkous, M.E. Piper, Z. Sickey, K. Zimmet, I. Mendoza, S. Suresh, E. Topsakal, Textile-based inkjet-printed RFIDs: Exploring wearable antennas in the real world [bioelectromagnetics], IEEE Antennas Propag. Mag. 66 (1) (2024) 50–62, http://dx.doi.org/10.1109/MAP.2023.3334671.
[98] K. Guerchouche, E. Herth, L.E. Calvet, N. Roland, C. Loyez, Conductive polymer based antenna for wireless green sensors applications, Microelectron. Eng. 182 (2017) 46–52, http://dx.doi.org/10.1016/j.mee.2017.08.007.
[99] P. He, J. Cao, H. Ding, C. Liu, J. Neilson, Z. Li, I.A. Kinloch, B. Derby, Screen-printing of a highly conductive graphene ink for flexible printed electronics, ACS Appl. Mater. Interfaces 11 (35) (2019) 32225–32234, http://dx.doi.org/10.1021/acsami.9b04589.
[100] H. Arun, Advancements in the use of carbon nanotubes for antenna realization, AEU - Int. J. Electron. Commun. 136 (2021) 153753, http://dx.doi.org/10.1016/j.aeue.2021.153753.
[101] L. Liu, Z. Shen, X. Zhang, H. Ma, Highly conductive graphene/carbon black screen printing inks for flexible electronics, J. Colloid Interface Sci. 582 (2021) 12–21, http://dx.doi.org/10.1016/j.jcis.2020.07.106.
[102] K. Arapov, E. Rubingh, R. Abbel, J. Laven, G. de With, H. Friedrich, Conductive screen printing inks by gelation of graphene dispersions, Adv. Funct. Mater. 26 (4) (2016) 586–593, http://dx.doi.org/10.1002/adfm.201504030.
[103] M. Rafiq, A. Imran, A. Rasheed, S. uz Zaman, A review on the manufacturing techniques for textile based antennas, J. Eng. Fibers Fabrics 19 (2024) 15589250241226585, http://dx.doi.org/10.1177/15589250241226585.
[104] P. Wang, M. Hu, H. Wang, Z. Chen, Y. Feng, J. Wang, W. Ling, Y. Huang, The evolution of flexible electronics: From nature, beyond nature, and to nature, Adv. Sci. 7 (20) (2020) 2001116, http://dx.doi.org/10.1002/advs.202001116.
[105] Z. Hui, L. Zhang, G. Ren, G. Sun, H.-D. Yu, W. Huang, Green flexible electronics: Natural materials, fabrication, and applications, Adv. Mater. 35 (28) (2023) 2211202, http://dx.doi.org/10.1002/adma.202211202.
[106] D. Tobjörk, R. Österbacka, Paper electronics, Adv. Mater. 23 (17) (2011) 1935–1961, http://dx.doi.org/10.1002/adma.201004692.
[107] P. Lopez-Iturri, R. Ruiz-Feliu, I.P. Guembe, H. Klaina, F.J.T. Frances, P. Martinez, I.N. Amado, E. Basarte, J. Morentin, A.G. Saenz, S. Santesteban, J. Bravo, J.I.O. Echeverria, F. Falcone, Implementation of a low-cost chipless RFID system with paper-based substrates printed tags for traceability applications in the packaging sector, IEEE Sens. J. 23 (13) (2023) 14923–14937, http://dx.doi.org/10.1109/JSEN.2023.3277630.
[108] Y. Xue, B. Hou, S. Wang, Y. Shang, B. Chen, Y. Ju, A highly sensitive paper-based chipless RFID humidity sensor based on graphene oxide, Sensors Actuators A 358 (2023) 114457, http://dx.doi.org/10.1016/j.sna.2023.114457.
[109] L. Makkonen, Young's equation revisited, J. Phys.: Condens. Matter. 28 (13) (2016) 135001, http://dx.doi.org/10.1088/0953-8984/28/13/135001.
[110] W.G. Whittow, A. Chauraya, J.C. Vardaxoglou, Y. Li, R. Torah, K. Yang, S. Beeby, J. Tudor, Inkjet-printed microstrip patch antennas realized on textile for wearable applications, IEEE Antennas Wirel. Propag. Lett. 13 (2014) 71–74, http://dx.doi.org/10.1109/LAWP.2013.2295942.
[111] B. Krykpayev, M.F. Farooqui, R.M. Bilal, M. Vaseem, A. Shamim, A wearable tracking device inkjet-printed on textile, Microelectron. J. 65 (2017) 40–48, http://dx.doi.org/10.1016/j.mejo.2017.05.010.
[112] S. Pacchini, M. Cometto, J.J. Chok, G. Dufour, N. Tiercelin, P. Pernod, T.B. Kang, P. Coquet, Inkjet-printing of hybrid Ag/conductive polymer towards stretchable microwave devices, in: 2015 European Microwave Conference, EuMC, 2015, pp. 865–868, http://dx.doi.org/10.1109/EuMC.2015.7345901.
[113] J.H. Lee, P.A. Dzagbletey, M. Jang, J.-Y. Chung, J.-H. So, Flat yarn fabric substrates for screen-printed conductive textiles, Adv. Eng. Mater. 22 (12) (2020) 2000722, http://dx.doi.org/10.1002/adem.202000722.
[114] H. Hong, J. Hu, X. Yan, Effect of the basic surface properties of woven lining fabric on printing precision and electrical performance of screen-printed conductive lines, Textile Res. J. 90 (11–12) (2020) 1212–1223, http://dx.doi.org/10.1177/0040517519888251.
[115] C. Aydemir, B.N. Altay, M. Akyol, Surface analysis of polymer films for wettability and ink adhesion, Color Res. Appl. 46 (2) (2021) 489–499, http://dx.doi.org/10.1002/col.22579.
[116] D.P. Ames, S.J. Chelli, Surface contamination effects on film adhesion on metals and organic polymers, Surf. Coat. Technol. 187 (2–3) (2004) 199–207, http://dx.doi.org/10.1016/j.surfcoat.2004.03.027.
[117] L. Huang, Y. Huang, J. Liang, X. Wan, Y. Chen, Graphene-based conducting inks for direct inkjet printing of flexible conductive patterns and their applications in electric circuits and chemical sensors, Nano Res. 4 (2011) 675–684, http://dx.doi.org/10.1007/s12274-011-0123-z.
[118] T. Huhtamaki, X. Tian, J.T. Korhonen, R.H. Ras, Surface-wetting characterization using contact-angle measurements, Nat. Protoc. 13 (7) (2018) 1521–1538, http://dx.doi.org/10.1038/s41596-018-0003-z.
[119] D. Soltman, V. Subramanian, Inkjet-printed line morphologies and temperature control of the coffee ring effect, Langmuir 24 (5) (2008) 2224–2231, http://dx.doi.org/10.1021/la7026847.
[120] M. Gilliam, Polymer surface treatment and coating technologies, in: Handbook of Manufacturing Engineering and Technology, Springer, 2015, pp. 99–124, http://dx.doi.org/10.1007/978-1-4471-4670-4_20.
[121] D.R. Joshi, N. Adhikari, An overview on common organic solvents and their toxicity, J. Pharm. Res. Int 28 (3) (2019) 1–18, http://dx.doi.org/10.9734/jpri/2019/v28i330203.

[122] M. Tobiszewski, S. Tsakovski, V. Simeonov, J. Namiesnik, F. Pena-Pereira, A solvent selection guide based on chemometrics and multicriteria decision analysis, Green Chem. 17 (10) (2015) 4773–4785, http://dx.doi.org/10.1039/C5GC01615K.

[123] K. Alfonsi, J. Colberg, P.J. Dunn, T. Fevig, S. Jennings, T.A. Johnson, H.P. Kleine, C. Knight, M.A. Nagy, D.A. Perry, et al., Green chemistry tools to influence a medicinal chemistry and research chemistry based organisation, Green Chem. 10 (1) (2008) 31–36, http://dx.doi.org/10.1039/B711717E.

[124] S. Kumar, V. Bhat, K.J. Vinoy, V. Santhanam, Using an office inkjet printer to define the formation of copper films on paper, IEEE Trans. Nanotechnol. 13 (1) (2013) 160–164, http://dx.doi.org/10.1109/TNANO.2013.2295765.

[125] S. Pranonsatit, D. Worasawate, P. Sritanavut, Affordable ink-jet printed antennas for RFID applications, IEEE Trans. Components, Packag. Manuf. Technol. 2 (5) (2012) 878–883, http://dx.doi.org/10.1109/TCPMT.2012.2186571.

[126] S.M. Bidoki, J. Nouri, A. Heidari, Inkjet deposited circuit components, J. Micromech. Microeng. 20 (5) (2010) 055023, http://dx.doi.org/10.1088/0960-1317/20/5/055023.

[127] D. Jang, D. Kim, J. Moon, Influence of fluid physical properties on ink-jet printability, Langmuir 25 (5) (2009) 2629–2635, http://dx.doi.org/10.1021/la900059m.

[128] N. Reis, C. Ainsley, B. Derby, Ink-jet delivery of particle suspensions by piezoelectric droplet ejectors, J. Appl. Phys. 97 (9) (2005) 094903, http://dx.doi.org/10.1063/1.1888026.

[129] R. Colella, A. Rivadeneyra, A.J. Palma, L. Tarricone, L.F. Capitan-Vallvey, L. Catarinucci, J.F. Salmeron, Comparison of fabrication techniques for flexible UHF RFID tag antennas [wireless corner], IEEE Antennas Propag. Mag. 59 (5) (2017) 159–168, http://dx.doi.org/10.1109/MAP.2017.2731214.

[130] R.D. Deegan, O. Bakajin, T.F. Dupont, G. Huber, S.R. Nagel, T.A. Witten, Capillary flow as the cause of ring stains from dried liquid drops, Nature 389 (6653) (1997) 827–829, http://dx.doi.org/10.1038/39827.

[131] D. Mampallil, H.B. Eral, A review on suppression and utilization of the coffee-ring effect, Adv. Colloid Interface Sci. 252 (2018) 38–54, http://dx.doi.org/10.1016/j.cis.2017.12.008.

[132] X. Gong, K. Huang, Y.-H. Wu, X.-S. Zhang, Recent progress on screen-printed flexible sensors for human health monitoring, Sensors Actuators A (2022) 113821, http://dx.doi.org/10.1016/j.sna.2022.113821.

[133] S. Tepner, N. Wengenmeyr, L. Ney, M. Linse, M. Pospischil, F. Clement, Improving wall slip behavior of silver pastes on screen emulsions for fine line screen printing, Sol. Energy Mater. Sol. Cells 200 (2019) 109969, http://dx.doi.org/10.1016/j.solmat.2019.109969.

[134] H.-W. Lin, C.-P. Chang, W.-H. Hwu, M.-D. Ger, The rheological behaviors of screen-printing pastes, J. Mater. Process. Technol. 197 (1–3) (2008) 284–291, http://dx.doi.org/10.1016/j.jmatprotec.2007.06.067.

[135] A. Sharma, C.-S. Cheon, J.P. Jung, Recent progress in electroless plating of copper, J. Microelectron. Packag. Soc. 23 (4) (2016) 1–6, http://dx.doi.org/10.6117/KMEPS.2016.23.4.001.

[136] T.-M. Wang, N.-W. Pu, Y.-M. Liu, W.-D. Chen, M.-D. Ger, W.-C. Lee, K.-S. Sun, Fabrication of RFID antennas on non-woven slag fiber paper, J. Taiwan Inst. Chem. Eng. 45 (1) (2014) 242–248, http://dx.doi.org/10.1016/j.jtice.2013.04.002.

[137] B.S. Cook, Y. Fang, S. Kim, T. Le, W.B. Goodwin, K.H. Sandhage, M.M. Tentzeris, Inkjet catalyst printing and electroless copper deposition for low-cost patterned microwave passive devices on paper, Electron. Mater. Lett. 9 (2013) 669–676, http://dx.doi.org/10.1007/s13391-013-3027-0.

[138] J.-J. Chen, G.-Q. Lin, Y. Wang, E. Sowade, R.R. Baumann, Z.-S. Feng, Fabrication of conductive copper patterns using reactive inkjet printing followed by two-step electroless plating, Appl. Surface Sci. 396 (2017) 202–207, http://dx.doi.org/10.1016/j.apsusc.2016.09.152.

[139] Y. Zhang, T. Zhang, H. Shi, Q. Liu, T. Wang, Fabrication of flexible copper patterns by electroless plating with copper nanoparticles as seeds, Appl. Surface Sci. 547 (2021) 149220, http://dx.doi.org/10.1016/j.apsusc.2021.149220.

[140] J.-Q. Xie, J. Tian, L. Mao, H. Cao, B. Zhou, L. Shi, S. Hou, Y. Ji, X.-Z. Fu, A facile and universally applicable additive strategy for fabrication of high-quality copper patterns based on a homogeneous ag catalyst ink, Chem. Eng. J. 477 (2023) 147115, http://dx.doi.org/10.1016/j.cej.2023.147115.

[141] Y. Farraj, A. Kanner, S. Magdassi, E-textile by printing an all-through penetrating copper complex ink, ACS Appl. Mater. Interfaces 15 (17) (2023) 21651–21658, http://dx.doi.org/10.1021/acsami.3c02242.

[142] C. Liu, S. Li, S. Wang, S. Luo, H. Zeng, D. Wang, Inkjet printing electroless copper plating on aluminum nitride substrate, Mater. Today Commun. 37 (2023) 107170, http://dx.doi.org/10.1016/j.mtcomm.2023.107170.

[143] Y. Mao, M. Zhu, W. Wang, D. Yu, Well-defined silver conductive pattern fabricated on polyester fabric by screen printing a dopamine surface modifier followed by electroless plating, Soft Matter 14 (7) (2018) 1260–1269, http://dx.doi.org/10.1039/C7SM02246H.

[144] M. Schlesinger, M. Paunovic, Modern electroplating, fifth ed., in: The electrochemical society series, (no. 52) Wiley, 2010.

[145] S.K. Dubey, P. Das, Formaldehyde: Risk assessment, environmental, and health hazard, in: J. Singh, R. Kaushik, M. Chawla (Eds.), Hazardous Gases, Academic Press, 2021, pp. 169–182, http://dx.doi.org/10.1016/B978-0-323-89857-7.00026-8.

[146] Y. Liao, S. Zhang, R. Dryfe, Electroless copper plating using dimethylamine borane as reductant, Particuology 10 (4) (2012) 487–491, http://dx.doi.org/10.1016/j.partic.2011.09.009.

[147] W. Zhang, D. Ding, Electroless copper plating on liquid crystal polymer films using dimethylamine borane as reducing agent, J. Chinese Chem. Soc. 63 (2) (2016) 222–228, http://dx.doi.org/10.1002/jccs.201500412.

[148] H. Hai, J. Ahn, D. Kim, J. Lee, H. Chung, C. Kim, Developing process for coating copper particles with silver by electroless plating method, Surf. Coat. Technol. 201 (6) (2006) 3788–3792, http://dx.doi.org/10.1016/j.surfcoat.2006.03.025.

[149] X. Xu, X. Luo, H. Zhuang, W. Li, B. Zhang, Electroless silver coating on fine copper powder and its effects on oxidation resistance, Mater. Lett. 57 (24–25) (2003) 3987–3991, http://dx.doi.org/10.1016/S0167-577X(03)00252-0.